Acoustic Attenuation in the Lower Cloud Layer of Venus

A Thesis

Presented to the

Graduate Faculty of the

University of Louisiana at Lafayette

In Partial Fulfillment of the

Requirements for the Degree

Master of Science

Adam J. Trahan

Spring 2018

Acoustic Attenuation in the Lower Cloud Layer of Venus

Adam J. Trahan

APPROVED:

Andi Petculescu, Chair Associate Professor of Physics	Gabriela Petculescu Associate Professor of Physics
Natalia A. Sidorovskaia Head and Professor of Physics	Mary Farmer-Kaiser Dean of the Graduate School

For Russell, Jäger, and my mother Nancy.

Acknowledgments

I would like to sincerely thank my supervisor Dr. Andi Petculescu for undertaking this journey with me. I would also like to thank Dr. Gabriela Petculescu for all of our discussions, academic and not. I would also like to thank the Physics Department for supporting me in in every way, and for pushing me to become a better person and scholar. I would also like to express my gratitude for the additional financial support provided by the Louisiana Space Consortium through the Graduate Student Research Assistance Program.

I would also like to thank Russell for believing in me when I did not believe in myself, for supporting me so I could focus on my research, and pushing me to continue when I felt like giving up. I would also like to thank Jäger, who lies at my feet even now, for the unconditional love.

Finally, I would like to thank Jay, Kyle, Peter, Sonny, and Henry, who suffered alongside me. Our paths crossed for a brief instance, and I am very glad they did.

Table of Contents

List of Tables

List of Figures

List of Abbreviations, Mathematical Symbols, and Notation

Superscripts

$\prime$	Perturbation term
p	Isobaric
v	Isochoric
m	Mixture quantity

Subscripts

β	Evaporation/Condensation process
ℓ	Liquid phase
η	Momentum transfer process
1	Sulfuric acid (H_2SO_4)
2	Water (H_2O)
3	Sulfur trioxide (SO_3)
c	Critical quantity
D	Molecular diffusion process
d	Dry ambient gas
g	Moist gas (Dry + Vapor)

o	Equilibrium value
p	Particle quantity
r	Reduced quantity
T	Thermal transfer process
v	Liquid vapor phase

Greek

α	Volume fraction
β	Evaporation parameter
χ	Mole fraction
δ_{ij}	Kronecker delta
η	Viscosity (Pa s)
γ	Adiabatic index
κ	Thermal Diffusivity $\left(\mathrm{m^2\,s^{-1}}\right)$
λ	Thermal Conductivity $\left(\mathrm{W\,m^{-1}\,K^{-1}}\right)$
μ^{dip}	Dipole moment (Debye)
ν	Kinematic viscosity $\left(\mathrm{m^2\,s^{-1}}\right)$
ω	Angular frequency $\left(\mathrm{rad\,s^{-1}}\right)$

ρ Density $\left(\mathrm{kg\,m^{-3}}\right)$

Σ Stress tensor (Pa)

τ Steady relaxation time (s)

θ Unsteady relaxation time (s)

ζ Bulk viscosity (Pa s)

Latin

C Specific heat $\left(\mathrm{J\,kg^{-1}\,K^{-1}}\right)$

c Ideal gas sound speed $\left(\mathrm{m\,s^{-1}}\right)$

D Deformation rate tensor $\left(\mathrm{s^{-1}}\right)$

f Rate of change of momentum per unit volume $\left(\mathrm{N\,m^{-3}}\right)$

j Rate of change of mass per unit volume $\left(\mathrm{kg\,s^{-1}m^{-3}}\right)$

L Latent heat $\left(\mathrm{J\,kg^{-1}}\right)$

q Rate of change of heat per unit volume $\left(\mathrm{J\,s^{-1}m^{-3}}\right)$

R Gas Constant $\left(8.314\ \mathrm{J\,mol^{-1}\,K^{-1}}\right)$

w Weight fraction

Mathematical Symbols

$\boldsymbol{\nabla}$ Gradient operator

∇^2 Laplacian operator

: Tensor Multiplication

Abbreviations

CC Clausius-Clapeyron Relation

ESA European Space Agency

EVE European Venus Explorer

HAVOC High Altitude Venus Operational Concept

LCPS Cloud Particle Size Spectrometer

NIMS Near-Infrared Mass Spectrometer

SVP Saturation Vapor Pressure

VEX Venus Express

Chapter 1: Introduction

The prospect of extraterrestrial living has fascinated mankind for centuries. In science fictional writings, cinema, and art, living off-Earth seems to be the next logical step in our quest to survive and satiate our curiosity, as a species. In the context of extraterrestrial living, NASA has published a proof of concept for a human presence on Venus. The study has shown that sending crewed airships for long-term missions in the upper troposphere of Venus is not only feasible but also potentially safer and less costly than putting people on Mars. These potential advantages stem from Venus having a thick atmosphere acting as a radiation shield and also from Venus's proximity to Earth. Furthermore, Venus's gravity is closer to Earth's, making human crews less prone to the deleterious effects of low gravity. The High Altitude Venus Operational Concept (HAVOC) [1], proposes to place manned airships within the upper cloud layer of Venus in order to study its atmosphere in situ. There is also a sustained interest in the deployment of instrumented balloons in Venus's atmosphere, just below the upper cloud layer, for long-duration in situ measurements.

On Earth, powerful events such as earthquakes or volcanic eruptions produce infrasonic waves that can travel over long distances, with relatively small attenuation. The ability to detect and quantify infrasonic arrivals in the middle atmosphere—as opposed to detection of ionospheric perturbations from orbit—is appealing because i) the influence of charged particles on the acoustic wavenumber can be neglected, ii) nonlinear effects like wave steepening and period lengthening are reduced, and iii) local effects of wind mean flow and gravity waves on wave propagation may be reduced if the

balloon is advected with the flow. In addition, the seismic-to-acoustic coupling at Venus' surface is nearly 70 times more efficient than on Earth because of the dense atmosphere; furthermore, the overall acoustic attenuation coefficient is quite small up to 80 km (see Petculescu [2]). Thus, even relatively weak sources can produce detectable signals.

The two principal factors affecting sound propagation are dispersion (via the dependence of sound speed on frequency) and absorption (via the attenuation coefficient). They are obtained, respectively, from the real and imaginary parts of the complex acoustic wavenumber. In order to understand and predict low-frequency acoustic propagation in the atmosphere of Venus, one must develop a model for the wavenumber for i) the cloudless (base) environment and ii) the aqueous H_2SO_4 clouds.

Acoustic wave propagation in the cloudless environment on Venus has already been investigated by Petculescu [2]. In this thesis, we provide predictions of the acoustic wavenumber, and thus the dispersion and attenuation, in the cloud layer of Venus (~50 km altitude). The effects of the cloud layer on low-frequency acoustic propagation will be based on a terrestrial model by Baudoin et al. [3]. In characterizing this process, the findings could potentially aid in the monitoring of sub-surface activity on the planet, or gain insight into lightning activity from lightning-generated infrasound.

1.1 Venus, a Brief History of Exploration

At altitudes below approximately 100 km, the lower atmosphere of Venus has a very dynamic and hostile environment. With average surface temperatures that are in excess of 730 K, and a dense atmosphere that exerts up to 95 bars of pressure [4], our

ability to perform in-situ surface measurements has been extremely limited. Regardless of the difficulty, spacecrafts from several nations have visited Venus.

In the 1970's, the Soviet Union's Venera spacecraft series (11-16) made the first landings on the surface of Venus. The probes took measurements of the planet's atmosphere during descent and were also able to transmit data from the surface for a short time. Evidence of lightning/thunder, surface wind speeds, soil samples, photographs, and temperature and pressure readings were reported back to Earth [5]. Then, between 1990 and 1994, NASA's Magellan mission used radar to map 98 percent of the planet's surface, and discovered that the planet's surface was volcanically and tectonically active, while also obtaining high resolution gravity data for 95 percent of the planet [5]. In 2006 the European Space Agency's (ESA) Venus Express (VEX) was sent to study the atmosphere of Venus, from the surface to the ionosphere [5]. From VEX radio occultation data, temperature and pressure profiles versus height were derived from neutral number density profiles [6]. Zonal and meridional wind measurements in Venus' cloud layer via image tracking (using images taken with the VIRTIS instrument [7]) was also determined. Currently, Japan's Akatsuki probe is studying Venus from orbit in order to better understand the atmospheric dynamics of the planet [8].

1.2 Lower Atmosphere and Cloud Layer

The ambient atmosphere of Venus is primarily composed of CO_2 (96.5%) and N_2 (3.5%). Other chemical species in trace amounts include, but are not limited to: small amounts of noble gases, water, and various sulfur compounds which are thought

to have resulted from volcanic activity [4]. Their respective abundances are shown in Table 1.1, [9].

Table 1.1. Chemical species and their relative abundances of Venus' ambient atmosphere.

Species	Volume Mixing Ratio
CO_2	0.965
N_2	0.035
O_2	0-20 ppm
SO_2	60 ppm
H_2O	50 ppm
Ar	70 ppm
CO	50 ppm

Venus' surface is extremely dense and hot, with average surface pressures of 92 bar and surface temperature of 735 K. Upwards into the atmosphere, temperature decreases and pressure falls, allowing the formation of clouds at particular altitudes. The vertical temperature and pressure profiles are shown in Figure 1.1 [6].

The entire planet is covered by clouds residing in a global layer that extends between 45 and 70 km altitude, approximately, with thinner hazes above and below. The bulk of the cloud layer is often referred to as the main cloud deck and is partitioned into three distinct layers: upper, middle, and lower. The partitions are based on in-situ probe measurements of distinctive cloud particle size distributions, and separated by regions of low particle number density [10].

The upper cloud layer lies between ~57-60 km and is produced photochemically. Below this, the middle (~57-50 km) and lower cloud (~50-45 km) layers are produced by condensation from vapor transported upward by convection via Hadley circulation

Figure 1.1. Vertical atmospheric temperature (left) and pressure (right) profiles for Venus. The global cloud layer lies within the horizontal dashed lines

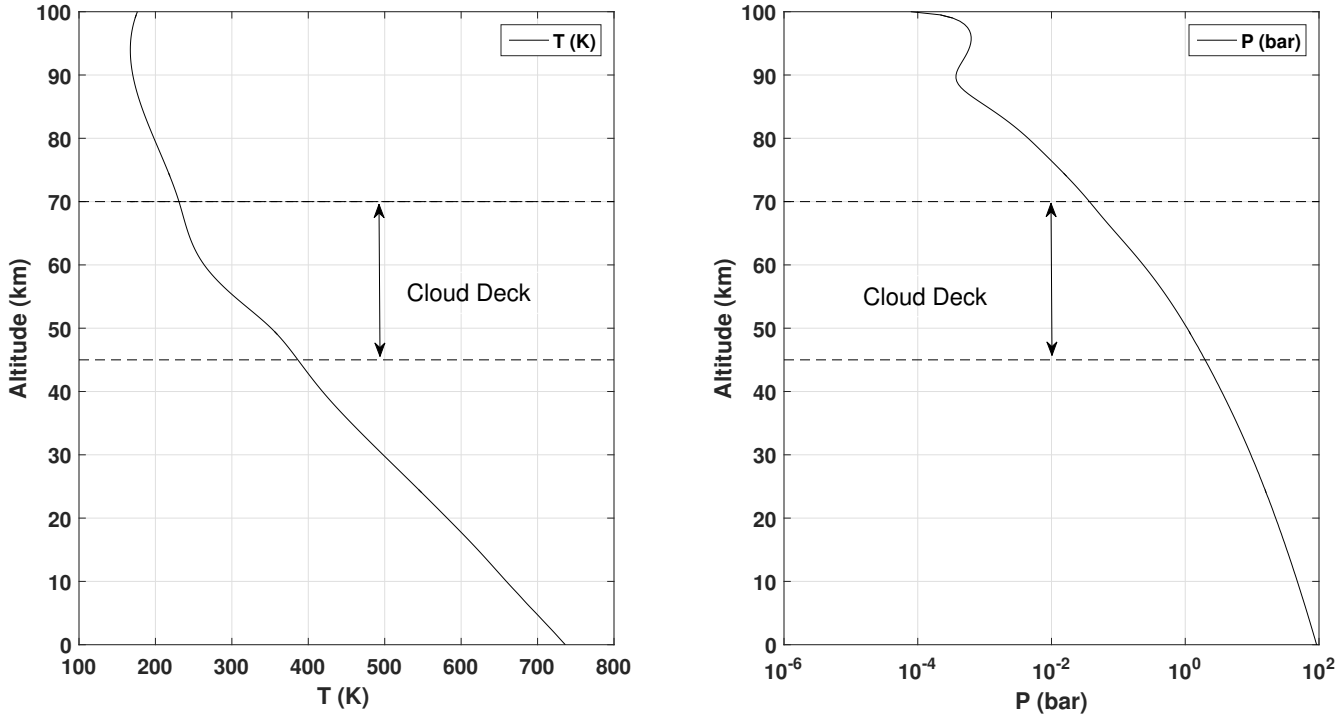

[11, 12]. While the atmosphere is relatively calm near the surface, retrograde zonal winds increase steadily up to 100 m/s at 60 km altitude [4]. These high westward winds are possibly the reason for the high spatial and temporal variability in cloud opacity, measured from infrared soundings from the Galileo spacecraft [13].

The clouds themselves are composed of aqueous sulfuric acid particles, $H_2SO_4 \cdot H_2O$, which are a binary mixture of sulfuric acid and water. The concentration of the sulfuric acid droplets was modeled by Imamura and Hashimoto [14], and varies within the cloud layers. The mole fraction is modeled to be $\chi_1 \approx 0.4$ in the upper cloud layer and $\chi_1 \approx 0.9$, in the middle and lower layers. Subscript 1 denotes H_2SO_4 while the subscript 2 will denote H_2O. The model results of Imamura and Hashimoto agree with

estimations from ground-based remote observations [15, 16, 17].

Measurements from the Pioneer Venus particle-size spectrometer indicate that the size distribution of the cloud particles contain three characteristic radii, called modes [18]. Mode 1 particles are the smallest mode and are found throughout the main cloud deck. Mode 2 particles are primarily located in the upper cloud layer and are produced by photochemical means [12]. Finally, mode 3 particles are found predominantly in the middle and lower cloud layer, and are the largest of all modes. There is still some disagreement regarding the composition of the mode 3 particles whether or not they are crystalline, the tail end of the mode 2 particle distribution, or a results of a measurement artifact [11].

Table 1.2. Average size of aqueous sulfuric acid particles by mode and their respective location in the cloud layers.

mode #	radii μm	cloud location
1	<0.3	ubiquitous
2	1.3	upper (57-60 km)
3	3.65	mid/lower (50-57/46-50 km)

Chapter 2: Model Review

2.1 Introduction to Acoustic Attenuation in Suspensions

The attenuation of a travelling acoustic wave in the atmosphere occurs by several mechanisms. Some of the first known mechanisms of acoustic absorption in an atmosphere are due to its viscous nature and its ability to conduct heat. These two mechanisms are referred to as classical absorption [19]. In addition to classical absorption, acoustic attenuation can also occur due to the transfer or redistribution of energy between translational and internal (molecular vibrational/rotational) modes [19]. In addition, the atmosphere may also contain a liquid phase, particles of which congregate to form clouds. The interplay between the two phases and hence their effects on atmospheric attenuation attenuation must be examined.

Acoustic propagation in a two-phase medium has been of interest since the early 20th century. The effects of phase changes on acoustic wave propagation in a liquid-gas mixture was studied by Gubaidullin and Nigmatullin. They considered the liquid phase as being composed of rigid spherical particles of varying size (polydisperse), suspended in a gaseous phase, which itself is also a mixture of the liquid's vapor phase and an inert gas. More recently, Baudoin et al. adapted the model of Gubaidullin and Nigmatullin for use in Earth's atmospheric clouds, a mixture of liquid water droplets, air, and water vapor. The presence of Earth clouds were predicted to play a significant role in the low frequency regime ($f \lessapprox 10$ Hz) [3].

The objective of this thesis is to give predictions of the complex acoustic wavenumber in the presence of clouds, by adapting the model of Baudoin et al. [3],

developed for Earth, to the Venusian atmosphere. The assumption of the model will first be examined in the context of Venus' atmosphere, then ambient, thermodynamic, and transport property data will be collected to complement the model. The key feature of clouds on Venus is that they are made of aqueous sulfuric acid particles, which is a binary *mixture* of sulfuric acid and water. This is in contrast to Earth clouds which are typically taken to be pure water in most of Earth's clouds, though sulfuric acid droplets certainly exist as an industrial by-product. Thus, various mixing rules will be employed in order to estimate thermodynamic and transport parameters which need to be considered in the model. Finally, the dependence of the attenuation coefficient and intrinsic dispersion on various cloud parameters will be investigated.

2.2 Model Description

The theoretical foundation of this research is given by Gubaidullin and Nigmatullin [20]. Theirs is a model which takes into account the effects of a two phase system on a traveling acoustic wave. The system consists of spherical liquid droplets suspended in a gaseous phase, which itself is a mixture of the liquid's own vapors, and an inert gaseous phase. For Venus, the liquid droplets are aqueous sulfuric acid ($H_2SO_4 \cdot H_2O$), and the inert gas is a combination of mostly carbon dioxide and nitrogen. The model considers four physical attenuation mechanisms: (1) viscoinertial effects, (2), heat transfer, (3) phase changes, and (4) vapor diffusion. Attenuation due to viscoinertial effects arises from the velocity mismatch between the liquid and gaseous phases. Heat transfer effects arise from temperature differences between the gas and liquid brought upon by compressions and expansions caused by the passing acoustic

wave. The local temperature deviations from thermal equilibrium caused by the acoustic wave,can also induce phase change. Phase changes may be limited by the diffusion of vapors produced at the droplet's surface into the ambient gas.

In order to calculate the attenuation and dispersion of plane acoustic waves in an aerosol, we consider the equations of continuity for the multiple phases. There are three distinct phases present; liquid, vapor, and dry atmosphere, which we shall assign the subscripts ℓ, v, and d, respectively. We can define a fourth phase as the combination of the dry and vapour phases, which we will term the gaseous phase and assign the subscript g. In the model, the presence of gravity and momentum exchanged during phase change is neglected. There is no heat source. The suspension is dilute and the liquid droplets are rigid spheres. The equations of continuity are:

$$\frac{\partial(\alpha_g \rho_g)}{\partial t} + \boldsymbol{\nabla} \cdot (\alpha_g \rho_g \mathbf{v}_g) = -j \tag{2.1}$$

$$\frac{\partial(\alpha_g \rho_v)}{\partial t} + \boldsymbol{\nabla} \cdot (\alpha_g \rho_v \mathbf{v}_g) = -j \tag{2.2}$$

$$\rho_{l0} \frac{\partial(\alpha_l)}{\partial t} + \rho_{l0} \boldsymbol{\nabla} \cdot (\alpha_l \mathbf{v}_\ell) = j \tag{2.3}$$

$$\alpha_g \rho_g \frac{D_g}{Dt}(\mathbf{v}_g) = -\mathbf{f} - \boldsymbol{\nabla} p_g + \boldsymbol{\nabla} \cdot \boldsymbol{\Sigma} \tag{2.4}$$

$$\alpha_l \rho_{l0} \frac{D_\ell}{Dt}(\mathbf{v}_\ell) = \mathbf{f} \tag{2.5}$$

$$\alpha_g \rho_g C^p_{g0} \frac{D_g}{Dt}(T_g) = \dot{q}_g + \lambda_{g0} \nabla^2 T + \boldsymbol{\Sigma} : \mathbf{D} \tag{2.6}$$

$$\alpha_l \rho_{l0} C_{l0} \frac{D_\ell}{Dt}(T_\ell) = \dot{q}_\ell \tag{2.7}$$

$$\dot{q}_g + \dot{q}_\ell = -j\, L \tag{2.8}$$

The first three equations, Equations (2.1)-(2.3), represent mass continuity for the gaseous (dry + vapor), vapor, and liquid phases, respectively. They tell us how the fluid's mass is changing in space and time by evaporation and condensation of the sulfuric acid. Following, Equations (2.4) and (2.5) represent the momentum conservation for the gaseous and liquid phase, respectively. Equations (2.6)-(2.8), represent the energy conservation for the gaseous and liquid phase, respectively. The final expression, Equation (2.8) represents the relationship between heat and mass exchange of the respective fluids as they are strongly coupled to one another through the process of evaporation and condensation. The subscripts $k = d, v, g, \ell$ represent the respective phases: dry atmospheric 'air', vapor, gaseous (vapor + dry atmosphere), and liquid. The symbols α_g and α_l represent the volume fraction of the gaseous and liquid phases, with $\alpha_g + \alpha_l = 1$. The symbols $\rho_k, P_k, T_k, \mathbf{v}_k$ represent the mass density, pressure, temperature, and velocity of the respective phase. The derivative $D_k/Dt = \partial_t + \mathbf{v}_k \cdot \nabla$ represents the convective derivative, and it is used for its respective phase. The strain rate tensor $\bar{\bar{\mathbf{D}}}$ and the stress tensor $\bar{\bar{\mathbf{\Sigma}}}$ are represented by the equations $\bar{\bar{\mathbf{D}}} = \frac{1}{2}\left[\boldsymbol{\nabla}\mathbf{v} + (\boldsymbol{\nabla}\mathbf{v})^T\right]$ and $\bar{\bar{\mathbf{\Sigma}}} = 2\eta_{g0}\bar{\bar{\mathbf{D}}} + (\zeta_{g0} - 2\eta_{g0}/3)(\boldsymbol{\nabla}\cdot\mathbf{v})\bar{\bar{\mathbf{I}}}$, with $\mathbf{v} = \alpha_g\mathbf{v_g} + \alpha_l\mathbf{v}_\ell$ representing the average velocity of the suspension, and η_{g0}, ζ_{g0} and λ_{g0} representing the dynamic shear viscosity, dynamic bulk viscosity and heat conductivity of the gaseous phase, respectively. C^p_{g0} and C_{l0} are the isobaric specific heat of the gaseous phase and the specific heat of the liquid phase. The tensor $\bar{\bar{\mathbf{I}}}$ is the unit 2nd-order tensor, $\bar{\bar{\mathbf{I}}} = \sum_{ij} \delta_{ij}\hat{\mathbf{e}}_i\hat{\mathbf{e}}_j$. Finally, the terms j, $\mathbf{f}$ and $\dot{q}$ represent the mass rate per unit volume due to phase change, the body force per unit volume applied to

the liquid particles, and the rate of change of heat per unit volume.

The velocity and temperature of a single liquid droplet, which we shall denote with a subscript p, depends on its size as well its location in space and time, that is $v_p = v_p(a, x, t)$ and $T_p = T_p(a, x, t)$. When the acoustic wavelength is sufficiently larger than the droplet spacing, a continuum formulation best describes the gaseous and liquid phases. Since the liquid phase of our system is composed of a discrete set of particles, the velocity and temperature fields describing the liquid phase can be represented as averages over all droplet sizes, $\mathbf{v}_\ell = \langle v_p(a, x, t)\rangle_a$ and $T_\ell = \langle T_p(a, x, t)\rangle_a$. The averaging mechanism by which the liquid fields are obtain are given by:

$$\langle g\rangle_a = \frac{\int_{a_{min}}^{a_{max}} V_p g(a) N(a) da}{\int_{a_{min}}^{a_{max}} V_p N(a) da}. \tag{2.9}$$

Here g is some function to be averaged, V_p is the particle volume, which we consider to be rigid spheres (i.e. $V_p = 4/3\pi a^3$), and $N(a)$ is the particle size distribution function. The averaging is taken over the limit of all particle sizes in the interval $[a_{min}, a_{max}]$. Outside of this range the distribution function is zero [20].

$$N(a) = \left\{ \begin{array}{ll} 0, & \text{for } a_{min} > a > a_{max} \\ N, & \text{for } a_{min} < a < a_{max} \end{array} \right\}$$

The term $N(a)da$ represents the number of particles per unit volume across some small region of radii $(a, a + da)$. Typically, but not exclusively, atmospheric droplet size distributions exhibit the same characteristic shape in many different types of clouds and meteorological conditions. Generally, the shape is that of a log-normal or gamma distribution, and can be modelled as such [21]. In this thesis, the log-normal distribution is used:

$$f(a|\mu, \sigma) = \frac{1}{a\sigma\sqrt{2\pi}} e^{-\frac{(ln(a)-\mu)^2}{2\sigma^2}}, \tag{2.10}$$

where a is the droplet radius and μ and σ are the parameters which describe the distribution. They and are not representative of the distribution's mean and variance [22].

From the distribution function, the total number of droplets per unit volume n, as well as the volume fractions for the gas and liquid phases, α_g and α_l, can be found through integration [20]:

$$n = \int_{a_{min}}^{a_{max}} N(a)da \tag{2.11}$$

$$\alpha_l = \int_{a_{min}}^{a_{max}} V_p N(a)da = \int_{a_{min}}^{a_{max}} \tfrac{4}{3}\pi a^3 N(a)da. \tag{2.12}$$

The volume fractions are related by the completion relation, $\alpha_g + \alpha_l = 1$. In general, the volume fraction of a mixture is defined as the ratio of constituent volume to the

total volume of the mixture (gaseous + liquid):

$$\alpha_i = \frac{V_i}{V} = \frac{V_i}{\sum_i V_i}. \tag{2.13}$$

The subscript i above pertains to all fluid phases: dry air, vapor, and liquid. Thus, $V = V_g + V_\ell$ in the above equation, is the total volume of the entire atmospheric mixture (i.e. gas and liquid phases).

The dispersion relation is obtained by first reducing the system of Equations (2.1) - (2.8) to one-dimension. The system is then linearized about equilibrium by assuming small plane wave disturbances. Letting $\psi(x,t)$ represent various state variables which describe the fluid (e.g. $\psi = p, \rho, T, v$ etc.), one can write, in the linear approximation,

$$\psi(x,t) \approx \psi_o + \psi'(x,t). \tag{2.14}$$

ψ_o denotes the equilibrium value while ψ' represents first-order acoustic perturbation, assumed much smaller than their equilibrium counterparts, i.e. $\psi' \ll \psi_o$. Further, since perturbation terms are assumed small, second-order perturbation terms (e.g. $P' \cdot \rho'$) are neglected.

All acoustic perturbations are considered to have plane wave solutions i.e.

$$\psi'(x,t) = \tilde{A}_\psi e^{i(\tilde{k}x - \omega t)}, \tag{2.15}$$

where $\tilde{A}_\psi$ is the complex wave amplitude in appropriate units, $\tilde{k} = k + ik^*$ is the complex wave number, and $\omega = 2\pi f$ is the angular frequency. It follows that

$$\psi'(x,t) = \tilde{A}_\psi e^{-k^* x} e^{i(kx-\omega t)}. \tag{2.16}$$

In this form we can clearly see that the perturbation term, ψ', decays exponentially with a decay constant equal to the imaginary part of the complex wavenumber k^*, containing attenuation effects.

The model further assumes all gaseous phases are ideal, the total pressure follows Dalton's law of partial pressure:

$$P = \sum_{i=1}^{n} P_i, \tag{2.17}$$

and the total mass of the gas is the sum of its constituent masses $\rho_g = \rho_d + \rho_v$. The saturation vapor pressure, P^{sat}, is related to the latent heat of evaporation/condensation L through the Clausius-Clapeyron (CC) equation:

$$\frac{\mathrm{d}P^{sat}}{\mathrm{d}T_d} = \frac{L\rho_v}{T_d} \tag{2.18}$$

Expressions for the flux terms of mass, momentum and energy flux are needed to fully specify and solve the system of equations presented above. The terms $j, f, \dot{q}$ are

provided by Gubaidullin and Nigmatullin [20]. First, expressions for the mass rate per unit volume j (in $\mathrm{kg\,m^{-3}\,s^{-1}}$) arise from equating the flux of evaporation given by the Hertz-Knudsen-Langmuir formula j_β, to the flux of diffusion of vapor through the air $j_\beta = j_D = j$ [3], with:

$$j_\beta = \alpha_{\ell o}\rho_{\ell o}\frac{r_o}{P_{go}}\left\langle \frac{P_v - P_\Sigma}{\tau_\beta}\right\rangle_a \tag{2.19}$$

$$j_D = \alpha_{\ell o}\rho_{\ell o}\frac{r_o}{P_{go}}\left\langle \frac{P_\Sigma - P^{sat}}{\tilde{\tau}_D}\right\rangle_a, \tag{2.20}$$

where j has been averaged over all droplet sizes. The terms $r_o = \rho_{go}/\rho_{\ell o}$ represent the ratio of densities, P_v and P_Σ are the vapor pressure and the vapor pressure reached just after evaporation, but before its diffusion in the inert gas, τ_β is the real time associated with phase changes and τ_D^* is the complex time associated with diffusion through the air. The average force per unit volume for a liquid particle moving within a viscous fluid can be represented as the sum of the viscous force due to Stokes's drag F_η, the Archimedes buoyant force F_A, the force of added-mass F_m and the Basset hereditary force F_B. The Stokes's Drag force of a spherical particle, suspended in a viscous medium, arises due to the relative velocity of that particle to the surrounding medium and is given by:

$$F_\eta = 6\pi\eta_g a(v_g - v_\ell) \tag{2.21}$$

The buoyant force arises from differences in particle density to the surrounding medium and is given by:

$$F_A = \frac{4}{3}\pi a^3 \rho_g \frac{\partial v_g}{\partial t} \tag{2.22}$$

The unsteady added-mass and Basset forces arise from; (1) as a particle accelerates through a viscous fluid, the surrounding fluid must be moved in order to accommodate the incoming particle, and thus imparts a retarding force, and (2) the need for the boundary layer to adapt to the new conditions as the particle is accelerated through the fluid. The added-mass and Basset forces are:

$$F_m = \frac{2}{3}\pi a^3 \rho_g \frac{\partial}{\partial t}(v_g - v_\ell) \tag{2.23}$$

$$F_B = 6a^2\sqrt{\pi \rho_g \eta_g} \int_{-\infty}^{t} \frac{\partial}{\partial \tau}(v_g - v_\ell)\frac{1}{\sqrt{t-\tau}} d\tau \tag{2.24}$$

The expression for the force per unit volume f (in $\mathrm{N\,m^{-3}}$) is given by:

$$f = \alpha_{\ell o}\rho_{\ell o}\left\langle \frac{v_g - v_\ell}{\tilde{\tau}_\nu} - \frac{v_g}{\tilde{\tau}_A} \right\rangle_a, \tag{2.25}$$

where f has been averaged across all droplet sizes. The force experienced by the particles is averaged across all droplets sizes and depends on the time it takes for the particle to respond to the acoustic wave forcing. Here $\tilde{\tau}_\nu$ is the complex time associated with the Stokes, Basset, and added-mass force, while $\tilde{\tau}_A$, is a complex time associated

to the Archimedes buoyant force. Similarly, the rates of change of heat per unit volume $\dot{q}$ (in $\mathrm{J\,m^{-3}\,s^{-1}}$) are obtained by solving the unsteady heat equation inside and outside the droplet surface with surface temperature T_Σ [20]:

$$\dot{q}_g = -\alpha_{go}\rho_{\ell o} r_o C_{go}^P \left\langle \frac{T_g - T_\Sigma}{\tilde{\tau}_{\Sigma_g}} \right\rangle_a \tag{2.26}$$

$$\dot{q}_\ell = -\alpha_{\ell o}\rho_{\ell o} C_{\ell o} \left\langle \frac{T_\ell - T_\Sigma}{\tilde{\tau}_{T_\ell}} \right\rangle_a . \tag{2.27}$$

The complex times $\tilde{\tau}_{\Sigma_g}$ and $\tilde{\tau}_{T_\ell}$ represent the relaxation times for heat conduction associated with the gaseous and liquid phases, respectively.

The various relaxation times which appear in the flux terms above arise naturally from their respective governing equations. They represent the time it takes for the medium to adjust to new equilibrium conditions imparted by the acoustic perturbations. Times marked with a tilde (e.g. $\tilde{\tau}$) are complex quantities while times without are real. τ denotes steady transfer times while θ denotes unsteady transfer times. The times are associated with the following processes:

- Momentum transfers

$$\tau_\nu = \frac{2}{9}\frac{\rho_{\ell o} a^2}{\rho_{go}\nu_{go}} \qquad \theta_\nu = \frac{a^2}{\nu_{go}}$$

$$\tilde{\tau}_\nu = \frac{\tau_\nu}{\left[1 - \frac{1}{9} i\omega\theta_\nu + \frac{1-i}{\sqrt{2}}\sqrt{\omega\theta_\nu}\right]} \qquad \tilde{\tau}_A = \frac{-i}{\omega r_o} \tag{2.28}$$

In the expressions above, $\nu_{go} = \eta_{go}/\rho_{go}$ represents the kinematic viscosity of the gas and r_o is the density ratio defined above. The three terms in $\tilde{\tau}_v$ correspond, respectively to Stokes drag, added-mass, and Basset forces (where τ_v is the real time associated with Stokes drag), and $\tilde{\tau}_A$ is associated with Archimedes buoyancy force. It can be seen that for the low frequency case, when $\omega \ll 1$, the relaxation time $\tilde{\tau_\nu} \approx \tau_\nu$. That is, the added-mass and Basset forces become negligible for low frequencies and the force on a particle is dominated by Stokes drag. The force due to added-mass becomes dominant for high frequencies $\omega \gg 1$, and added-mass and Basset forces are important for intermediate frequencies.

- Heat transfer in gaseous phase

$$\begin{aligned} \theta_{T_g} &= \frac{a^2}{\kappa_{go}} & z_g &= \frac{1-i}{\sqrt{2}}\sqrt{\omega\theta_{T_g}} & \eta_g &= \frac{1}{1+z_g} \\ \tau_T &= \frac{1}{3}\frac{\rho_{\ell o}a^2}{\rho_{go}\kappa_{go}} & \tau^*_{T_g} &= \frac{1}{3}\theta_{T_g}\eta_g & \tilde{\tau}_{\Sigma_g} &= \frac{\alpha_{go}}{\alpha_{go}}\tau^*_{T_g} \end{aligned} \tag{2.29}$$

- Heat transfer in liquid phase

$$\begin{aligned} \theta_{T_\ell} &= \frac{a^2}{\kappa_{go}} & z_\ell &= \frac{1-i}{\sqrt{2}}\sqrt{\omega\theta_{T_\ell}} \\ \eta_\ell &= \frac{5[3z_\ell(3+z_\ell^2)\tanh(z_\ell)]}{z_\ell^2(\tanh(z_\ell)-z_\ell)} & \tilde{\tau}_{T_\ell} &= \frac{1}{15}\theta_{T_\ell}\eta_\ell \end{aligned} \tag{2.30}$$

where the parameters $\kappa_{go} = \lambda_{go}/\rho_{go}C^p_{go}$ and $\kappa_{\ell o} = \lambda_{\ell o}/\rho_{\ell o}C^p_{\ell o}$. The relaxation time τ_T being the time associated with steady heat transfer in the absence of phase-change effects.

- Vapor diffusion in air

$$\theta_D = \frac{a^2}{D} \qquad z_D = \frac{1-i}{\sqrt{2}}\sqrt{\omega\theta_D} \qquad \eta_D = \frac{1}{1+z_D}$$
$$\tau_D = \frac{1}{3}\frac{\rho_{\ell o}a^2}{\rho_{go}D} \qquad \tilde{\tau}_D = \frac{1}{3}\frac{R_v}{R_g}(1-k_{vo})\theta_D \tag{2.31}$$

The parameters D and $R_{v/g}$ represent the binary diffusion coefficient and the specific gas constant for the vapor/gas phase, respectively, while $k_{vo} = \rho_{vo}/\rho_{go}$ represents the specific humidity.

- Evaporation and condensation

$$\tau_\beta = \frac{1}{3}\sqrt{\frac{2\pi}{\gamma_v}}\frac{\gamma_g c_{vo} a}{\beta c_{go}^2} \tag{2.32}$$

The parameters γ_k and $\mathrm{c_{ko}} = \sqrt{\gamma_\mathrm{k}\mathrm{R}_\mathrm{k}^*\mathrm{T}}$ are the adiabatic index and ideal sound speeds for phase k and β is the evaporation coefficient of water, found in the Hertz-Knudsen-Langmuir formula.

Acoustic attenuation and dispersion can also be framed in the context of the relaxation times. A gas-vapor-liquid system perturbed from equilibrium will adapt to the new conditions in order to reacquire equilibrium. It has been shown that for momentum and thermal transfers, the attenuation peaks around the values $\omega\tau_\nu \approx 1$ and $\omega\tau_T = \approx 1$, respectively [23]. For phase change effects, the attenuation is dependent upon the amount of liquid present. Thus, the attenuation peak is maximum near $\omega\tau_D \approx m$, where $m = \alpha_{\ell o}\rho_{\ell o}/\alpha_{go}\rho_{go}$ is the quantity of liquid droplets [24, 25]. For each

relaxation time τ, one can associate a characteristic frequency. These characteristic frequencies correspond to the locations of maximum attenuation, and are defined in Table 2.1.

The relaxation time for momentum transfers is on the order of 10^{-4} s, which corresponds to a characteristic frequency of $f_\nu = 500$ Hz. Thus attenuation due to momentum exchanges should be maximum in this region. Thermal transfers are maximum in the kHz region. Attenuation due to phase changes brought upon by the acoustic wave is influenced by two relaxation times. The first is the time taken for a liquid droplet to evaporate/condense, which occurs quite rapidly, on the order of 10^{-10} s. The second relaxation time to influence phase changes is the the time it takes for recently evaporated vapors to diffuse into the surround ambient gas, which occurs on time scales on the order of 10^{-4} s, much slower than the evaporation time. Thus, the particle is able to evaporate much more rapidly than the vapor is able to diffuse into the atmosphere and thus a buildup of vapor occurs on the droplet surface, saturating the local space and slowing the evaporation process. This is reflected in the characteristic frequencies of evaporation/condensation f_β and diffusion f_D.

Table 2.1. Relaxation times for momentum transfer τ_ν, thermal transfers τ_T, vapor diffusion τ_D, and evaporation/condensation τ_β and their respective characteristic frequencies.

-	Order (sec.)	Frequency	freq.(Hz)	Transfer Type
τ_ν	10^{-4}	$f_\nu = 1/(2\pi\tau_\nu)$	500	Momentum
τ_T	10^{-5}	$f_T = 1/(2\pi\tau_T)$	1,000	Thermal
τ_D	10^{-4}	$f_D = m/(2\pi\tau_D)$	0.02	Diffusion
τ_β	10^{-10}	$f_\beta = 1/(2\pi\tau_\beta)$	10^9	Eva./Cond.

2.3 Dispersion Relation

The dispersion relation for our plane waves solutions takes on the form:

$$k(\omega) = \frac{\omega}{c_{go}}\sqrt{V(\omega)D(\omega)}, \tag{2.33}$$

where

$$\begin{aligned} V(\omega) &= 1 + mX_1(\omega) \\ D(\omega) &= 1 + mX_2(\omega) \end{aligned}$$

and

$$X_1(\omega) = \frac{(\alpha_{go} - r_o)\left\langle h_F \right\rangle_a - \alpha_{go} r_o}{1 + m r_o \left\langle h_F \right\rangle_a}$$

$$X_2(\omega) = (\gamma_{go} - 1)\frac{\left\langle h_{T2} \right\rangle_a - \bar{R}_v k_{vo}\gamma_{go}\left(\bar{R}_v \bar{C}^P_{go}\left\langle h_{T3} \right\rangle_a - 2\bar{L} r_o \left\langle h_{T1} \right\rangle_a - M_1\Lambda\right)}{1 + m(\left\langle h_{T2} \right\rangle_a - B\left\langle h_{T3} \right\rangle_a - M_2\Lambda)}.$$

Both functions $V(\omega)$ and $D(\omega)$ are functions of the acoustic wave frequency, hidden in the relaxaion times, as well as many thermodynamic variables. The function $V(\omega)$ represents the contributions of momentum transfers, and $D(\omega)$ represents the contributions of thermal and mass transfer. They are of the form $1 + m$, where $m = \dfrac{\alpha_{\ell o}\rho_{\ell o}}{\alpha_{go}\rho_{go}}$ is the liquid mass fraction, as effects induced by the presence of liquid droplets are proportional to the concentration of the liquid droplets.

2.4 Model Assumptions

The model relies on a number of simplifying assumptions. Below, I provide a semi-quantitative discussion of these assumptions.

The ideal gas assumption. Each gas phase species is considered to obey the ideal gas law,

$$P_i = \rho_i R_i^* T_g, \tag{2.34}$$

where $R_i^* = R/M_i$ is the specific gas constant with M being the molar mass, and $i = v, d, g$. This assumption is validated by the compressibility factor of the gas $P/\rho R^* T$; deviations of this quantity from 1 is a measure of how much the gas differs from ideal. Figure 2.1 gives the compressibility factor of the ambient atmosphere on Venus versus altitude. Within the cloud deck the maximum deviation is near the upper cloud (~67 km) and of the order of 5%. Above the cloud deck the compressibility factor becomes quite large with altitude.

Figure 2.1. Ambient gas compressibility versus altitude. Within the cloud layer the maximum deviation is in the upper cloud layer(of ~5%)

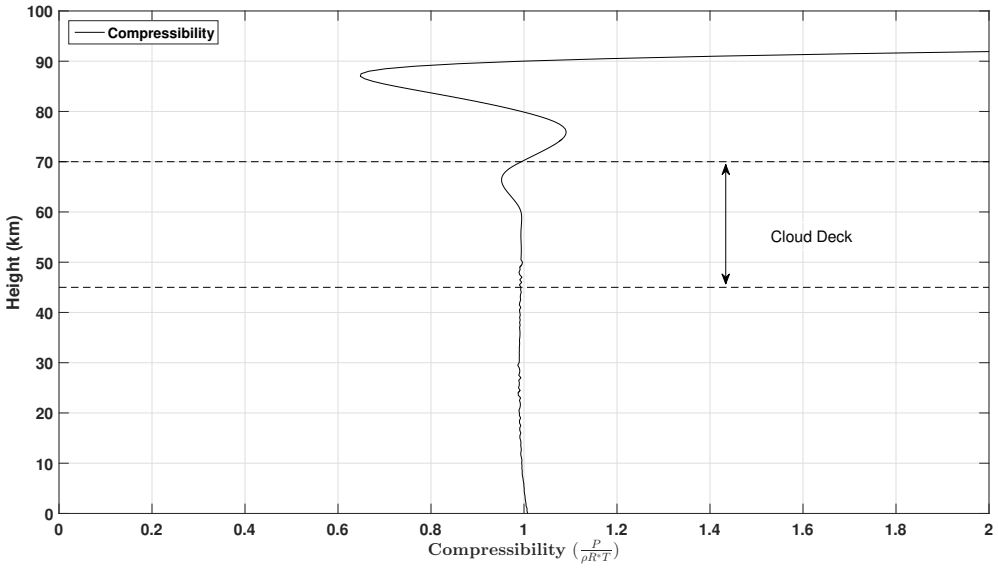

The continuum approximation. The upper troposphere of Venus is treated as a continuum, via the Navier-Stokes-Fourier equations. In the literature, the problem of when a medium can be considered continuous or not is somewhat diffuse and subjective. The answer lies in how many collisions occur between particles in a certain characteristic time (e.g. the acoustic period) or, equivalently, how the mean-free-path compares to a characteristic length (e.g. the acoustic wavelength). The parameter that is used typically to establish the "continuity" of a medium is the Knudsen number, Kn, defined as the ratio of the molecular mean free path to a representative length scale:

$$\mathrm{Kn} = \frac{\ell}{L}, \tag{2.35}$$

where ℓ is the molecular mean free path and L is a characteristic length. A fluid is

assumed to diverge from a continuum, to the point that the Navier-Stokes-Fourier theory starts to fail, when Kn > 0.1 An estimate for the Knudsen number in the cloud layer, using the cloud particle size as the characteristic length i.e. $L = a$, is $\mathrm{Kn} = \eta_{\mathrm{go}}/\rho_{\mathrm{go}}\mathrm{c}_{\mathrm{go}}\mathrm{a}$. Values for η_{go} and ρ_{go} are given in Table 3.8, $c_{go} = \sqrt{\gamma_g R_g^* T_g}$ is the ideal gas sound speed, and a is the mean cloud droplet size (modes). The Knudsen numbers for the three modes are given in Table 2.2. The values lie within the range $0.010 \leq \mathrm{Kn} \leq 0.13$. Thus, there are roughly ten gas particle collisions per mode-1 particle and 100 collisions per mode-3 particles. In this region the Navier-Stokes-Fourier equations still describe the flow adequately, with some reservations.

Table 2.2. Knudsen numbers for various modes.

Mode (μm)	1 ($a = 0.3$)	2 ($a = 1.3$)	3 ($a = 3.65$)
Kn	0.13	0.038	0.010

Since we are free to choose the representative length scale L, one can define an acoustic Knudsen number $\mathrm{Kn}^{\mathrm{ac}}$:

$$\mathrm{Kn}^{\mathrm{ac}} = \frac{\ell}{\lambda}, \tag{2.36}$$

in which ℓ is still the gas mean free path length and λ represents the acoustic wavelength. An approximation for the acoustic Knudsen number is the same as before:

$$\mathrm{Kn}^{\mathrm{ac}} = \left(\frac{\eta_{\mathrm{go}}}{\rho_{\mathrm{go}}\mathrm{c}_{\mathrm{go}}}\right)\frac{1}{\lambda} = \left(\frac{\eta_{\mathrm{go}}}{\rho_{\mathrm{go}}\mathrm{c}_{\mathrm{go}}^2}\right)\mathrm{f}. \tag{2.37}$$

where the relation $c = \lambda f$ was used. For the frequency interval 0.01 Hz $< f <$ 10 kHz, we obtain acoustic Knudsen numbers in the range of $1.3 \times 10^{-13} <$ Kn $< 1.3 \times 10^{-6}$. Thus the continuum approximation is well satisfied for the acoustic Knudsen number. In fact, to satisfy $\mathrm{Kn}^{\mathrm{ac}} < 0.1$, we are bounded to the frequency region less than about 100 MHz, which is 10^4 times larger than the largest frequency used in the model.

The dilute-suspension approximation. The model also assumes the suspension is dilute in order to neglect droplet-droplet interactions. Thus, the volume fraction α_l of the liquid phase must necessarily be small. The volume fraction can be estimated from the cloud density ρ_{cl} (mass of condensate per total volume). The cloud density is introduced in section 3.3, and has a value of $\rho_{cl} \approx 4.5 \times 10^{-5} \mathrm{kg\,m^{-3}}$. This value represents the maximum cloud density with no precipitation or other cloud dynamics and whose real value lies between 1–100% of ρ_{cl}. At most, (100% ρ_{cl}), the estimate for the volume fraction occupied by the liquid phase is $\alpha_l = \rho_{cl}/\rho_{\ell o} \approx 2 \times 10^{-8} \ll 1$, where ρ_{lo} is the mass density of the liquid phase which is given in Table 3.3. In reality, α_l will be smaller and thus satisfies the dilute approximation.

The plane-wave assumption. Acoustic waves are assumed to be plane waves in the model. The validity of this assumption depends upon the scale on which the ambient parameters (e.g. temperature, density, pressure, composition etc.) change with respect to an acoustic wavelength. Hence, in the context of this model, as long as the cloud properties do not change appreciably with height or, equivalently, the wavelengths of interest are smaller than vertical cloud inhomogeneities, the plane-wave assumption should be a reasonable premise.

Chapter 3: Determination of Model Parameters

3.1 Ambient Atmospheric Parameters

In order to complete the model, atmospheric data must be gathered to satisfy the temperature-pressure dependence of the input parameters in the cloud region. Mixture rules must also be used in order to account for the multi-species condensates and vapor phases. Ambient temperature and pressure profiles are based on averaged values of VEX measurements taken from Tellmann et al. [6]. Thermophysical and transport parameters (specific heats, viscosities, thermal conductivities, and binary diffusion coefficients) of the pure species are obtained/calculated from a variety sources. Parameters for pure water are obtained mostly from Pruppacher and Klett [21]. Those of sulfuric acid, carbon-dioxide and nitrogen, are taken from the NIST Chemistry Webbook [26], Daubert et al. [27], and Poling et al. [28]. Cloud particle size characteristics are obtained from James et al. [13]. The saturation vapor pressure of pure sulfuric acid is taken from Ayers et al. [29] and Kulmala and Laaksonen [30]. Cloud density and atmospheric composition is taken from Sanchez-Lavega [9]. The cloud droplet acid composition is taken from Imamura and Hashimoto [12, 14]. Partial vapor pressures above the liquid phase are obtained from Gmitro and Vermeulen [31]. Additional consideration must be taken to account for the aqueous sulfuric acid condensate ($H_2SO_4 \cdot H_{20}$). Mixture rules are mostly found in Poling et al. [28].

The entire cloud deck lies approximately in the altitude range of $45 \text{ km} \leq z \leq 70 \text{ km}$. This corresponds to an ambient temperature and pressure range of $386 \text{ K} \leq T_d \leq 230 \text{ K}$ and $1.98 \times 10^{-1} \text{ MPa} \leq P_d \leq 3.69 \times 10^{-3} \text{ MPa}$, respectively, and

an atmospheric density of $2.693\ \mathrm{kg\,m^{-3}} \leq \rho_d \leq 8.393 \times 10^{-2}\ \mathrm{kg\,m^{-3}}$. A representative altitude of $z = 50$ km, and its respective temperature and pressure, is selected as input for all model parameters. This altitude has been chosen for several reasons. First, the empirical formula which gives the thermal conductivity of liquid sulfuric acid is only valid in the temperature range $273.59\ \mathrm{K} \leq T \leq 371.32\ \mathrm{K}$, which corresponds to the altitude range of ~48-59 km. This is the most narrow temperature region of all the parameters, and thus sets a boundary for our model. Second, the concentration (mole fraction) of sulfuric acid in the cloud droplets is roughly constant below ~50 km ($\chi_1 \approx 0.9$) [14, 12]. Third, all three modes are present in the middle and lower cloud layer (46-57 km altitude). This allows us to investigate the effects of the mean droplet size on the absorption and sound speed at a single height (i.e. a single temperature-pressure) . Finally, the European Space Agency and NASA are considering floating platforms such as aerostats (European Venus Explorer, or EVE) and even manned airships (HAVOC) cruising at this elevation. The presence of strong zonal winds in this region will be utilized as a form of transport around the planet [1, 32]. The ambient temperature, pressure, atmospheric density and cloud droplet concentration at $z = 50$ km are given in Table 3.1 [6, 14].

Table 3.1. Ambient parameters used for model input at an altitude of $z = 50$ km. χ_1 is the mole fraction of sulfuric acid inside the liquid droplet at the given height.

z (km)	T_d (K)	P_d (MPa)	ρ_d ($\mathrm{kg\,m^{-3}}$)	χ_1
50	351.5	0.107	1.594	0.9

Values for the evaporation coefficient β is largely unknown with little agreement in the literature. Values for water have been reported in the range from $\beta = 0.01$ to $\beta = 1$. Baudoin et al. [3] evaluate its significance within the context of their model. Their results show that for two orders of magnitude of change in β (from 0.01-1), the change in the attenuation coefficient is less than one order of magnitude. Thus the value $\beta = 1$, chosen in their work, is also adopted here. A historical review of the parameter is given by Eames et al. [33].

3.2 Particle Size Distribution Function

In clouds a variety a particle sizes are encountered resulting from various mechanisms of droplet growth (i.e. evaporation/condensation or collision and coalescence). The particle sizes can be described by a statistical distribution denoted by $N(a)$. On Earth, under a variety of meteorological conditions, the size distribution can be approximated with a log-normal or gamma distribution, as well as empirical ones [21]. As for Venus, a majority of the size distributions found in the literature are log-normal [18, 34, 35], and will thus be used in this thesis.

The log-normal distribution is given by the formula

$$N(a|\mu,\sigma) = \frac{1}{a\sigma\sqrt{2\pi}} e^{-\frac{(ln(a)-\mu)^2}{2\sigma^2}}, \tag{3.1}$$

where a is the droplet radius and μ andσ are the parameters which describe the distribution and are not representative of the distribution's mean and variance [22]. The mean and variance for the log-normal are functions of the parameters μ and σ:

$$\begin{aligned} mean &= e^{\mu+\sigma^2/2} \\ var &= e^{\left(2\mu+\sigma^2\right)}(e^{\sigma^2}-1). \end{aligned} \tag{3.2}$$

Inversely, the parameters μ and σ can be found if the distributions mean and variance are known:

$$\begin{aligned} \mu &= ln\Big(mean^2/\sqrt{var+mean^2}\Big) \\ \sigma &= \sqrt{ln(1+var/mean^2)} \end{aligned} \tag{3.3}$$

Measurements taken by the Pioneer Venus cloud particle size spectrometer (LCPS) show that the size distributions are multimodal in all cloud regions[18, 34] see Table 1.2. Inputs for the log-normal particle size distribution are taken from Grinspoon et al. [34] and shown in Table 3.2.

Table 3.2. Average particle sizes and their respective standard deviations taken from Grinspoon et al. Each mean value is obtained from a log-normal distribution.

Mode	Mean radius $\overline{a}(\mu m)$	std. dev.
1	0.3	1.56
2	1.0	1.29
3	3.65	1.28

3.3 Cloud Density and Volume Fractions

The density of the cloud is given as the ratio of the condensate mass to the total atmospheric volume. Approximate values for cloud density ρ_{cl} are obtained from Sánchez-Lavega et al. [36]. At the height of ~50 km, the cloud density is calculated to be $\rho_{cl} = 4.5 \times 10^{-5}\ \mathrm{kg\,m^{-3}}$. This value is represents the maximum possible cloud density in the absence of cloud dynamics and precipitation. In reality, the cloud density is highly variable. Measurements made by the the Galileo Near-Infrared Mapping Spectrometer (NIMS) revealed thick opaque cloud regions beside bright cloudless spots [34]. Hence, Sánchez-Lavega recommends multiplying ρ_{cl} by a factor ranging from 0.01 to 1. As no particularly value is recommended, a default value of 0.8 is used. The effects of varying cloud density on the attenuation and dispersion is examined in Chapter 4.

3.4 Thermodynamic Parameters

The liquid density of the sulfuric acid is well known and can be found readily from a multitude of sources. On the other hand, the vapor density is somewhat more difficult to obtain. The vapor phase above sulfuric acid is composed of water, sulfuric acid, and sulfur trioxide from the dissociation of the acid [31]:

$$\mathrm{H_2SO_4}(g) = \mathrm{H_2O}(g) + \mathrm{SO_3}(g) \tag{3.4}$$

The partial vapor pressures of sulfuric acid, water, and sulfur trioxide above aqueous sulfuric acid are calculated as functions of acid concentration at various temperatures by Gmitro and Vermeulen [31]. From pure component partial vapor pressure data, the

respective densities can be obtained through the ideal gas law (2.34). At the altitude $z = 50$ km, the acid concentration (in mole fraction) of the liquid droplets are $\chi_1 = 0.9$. This corresponds to a concentration by weight of approximately $w_1 \approx 0.98$, which is obtained through the relation:

$$\chi_i = w_i \frac{\overline{M}}{M_i}, \tag{3.5}$$

where M_i and $\overline{M}$ represent the molar mass of component i, and the mean molar mass (defined in section 3.6). The pure component densities and partial vapor pressures for our given temperature and weight fraction are presented in Table 3.3.

Table 3.3. Calculated vapor densities from partial pressures and specific gas constants.

Component (i)	ρ_{iv} $\times 10^{-4}(\mathrm{kg\,m^{-3}})$	P_{iv} (Pa)	R_i^* ($\mathrm{J\,kg^{-1}\,K^{-1}}$)
1 (H_2SO_4)	2.24	6.66	84.78
2 (H_2O)	1.64	26.66	461.40
3 (SO_3)	0.018	0.067	103.84
Total	3.90	33.39	

The density and partial pressure of sulfur trioxide vapor is smaller by at least two orders of magnitude compared to water and sulfuric acid. Thus, contributions from sulfur trioxide could be ignored for simplicity. The total density and pressure of the vapor phase, ρ_v and P_v, respectively, is the sum of its components. Their values are given in the last row of Table 3.3.

3.4.1 Latent heat. One of the more difficult parameters to obtain is the latent heat of evaporation L. For water, it is given in Pruppacher et al. [21] by the formula:

$$L_{water} = 597.3\left(\frac{273.15}{T}\right)^{g}, \tag{3.6}$$

where

$$g = 0.167 + \left(3.67 \times 10^{-4}\right)T. \tag{3.7}$$

As for sulfuric acid, the latent heat is found through the use of the Clausius-Clapeyron (CC) relations and the saturation vapor pressure (SVP). The CC relation relates the slope of a phase boundary line of a single chemical species on a pressure-temperature curve to the latent heat. The Clausius-Clapeyron equation is given by:

$$\frac{\mathrm{d}P^{sat}}{\mathrm{d}T_d} = \frac{L}{T_d \Delta v}. \tag{3.8}$$

The parameters $P^{sat}, T_d, L,$ and v represent the saturation vapor pressure, droplet surface temperature, latent heat, and specific volume (inverse density) respectively, with $\Delta v = v_v - v_l$. Since we are considering a liquid-gas system, the specific volume of the vapor phase is much larger than that of the liquid which implies $\Delta v \approx v_v = (\rho_v)^{-1}$, and thus we obtain the relation given in Equation (2.18):

$$\frac{\mathrm{d}P^{sat}}{\mathrm{d}T_d} = \frac{L\rho_v}{T_d}.$$

The SVP is the pressure at which the fluxes of evaporation and condensation are equivalent (in equilibrium). The saturation vapor pressure of sulfuric acid is given as functions of temperature and mole fraction of the $H_2SO_4 \cdot H_2O$ solution,

$$ln\ P^{sat}(T, \chi_{acid}) = ln\ P_1^{sat}(T) + \frac{\mu_1^m(T, \chi_{acid}) - \mu_1(T)}{RT}. \tag{3.9}$$

The first term on the right is the natural logarithm of the SVP for pure sulfuric acid, while the second term, $\mu_1^m - \mu_1$, represents the difference between the chemical potential of the mixture and the pure component chemical potential, and R the universal gas constant. Data for the relative chemical potential is tabulated in Zeleznik [37].

Measurements of the SVP of sulfuric acid was taken by Ayers et al. [29] in the temperature region 338-445 K. Kulmana and Luuksanen [30] theoretically derived an expression for the SVP, and expanded the temperature range to larger values than that used by Ayers. The expressions for the SVP is given as,

$$ln\ P_1^{sat}(T) = 16.259 - \frac{10156}{T} + 7.42\left(1 + ln\ \frac{T_o}{T} + \frac{T_o}{T}\right), \tag{3.10}$$

where P_1^{sat} has units of bars, T in kelvin, and $T_o = 385$ K. With the temperature dependence of P_1^{sat} known, it is possible to evaluate the derivative on the left side of the CC relationship with some reservations. Since the temperature dependence of the relative chemical potential is unknown, it is assumed that it does not change

appreciably with a small change in temperature and is treated as constant. Additionally, since we constrained the model to altitudes below 50 km where the mole fraction is almost constant, the change in concentration with temperature (altitude) is negligible. This assumption allows us to evaluate the derivative of Equation (3.9).

Evaluating the derivative of (3.9), an expression for the specific latent heat L can be obtained,

$$L = \frac{T_d}{\rho_v} \frac{\mathrm{d}P^{sat}}{\mathrm{d}T_d} \tag{3.11}$$

For the ambient temperature and pressure at $z = 50$ km, the relative chemical potential is $(\mu^m - \mu)/RT = -0.3779$ and the density of the vapor phase is given in Table 3.3). A value of $L \approx 1.66 \times 10^4\,\mathrm{J\,kg^{-1}}$ is calculated for the model.

3.4.2 Specific heat. Values for the gaseous isobaric specific heat are given by a polynomial expansion in terms of temperature from various sources. The three equations below are used.

$$C^p(t) = a + bt + ct^2 + dt^3 + e/t^2, \tag{3.12}$$

$$C^p(T) = (a + bT + cT^2 + dT^3 + eT^4) \cdot R \tag{3.13}$$

$$C^p(T) = a + b\left[\frac{(c/T)}{sinh(c/T)}\right]^2 + d\left[\frac{(e/T)}{cosh(e/T)}\right]^2 \tag{3.14}$$

where a-e are constants, and t represents a modified temperature, $t = T/1000$, with T

in kelvins, and $R = 8.314\ \mathrm{J\,mol^{-1}\,K^{-1}}$ is the specific gas constant. Table 3.4 denotes which heat capacity equation is used for each gaseous species, their respective valid temperature ranges, and coefficient values.

Table 3.4. Constants for Equations (3.12) - (3.14).

Species	$\mathbf{N_2}$	$\mathbf{H_2O}$	$\mathbf{CO_2}$	$\mathbf{H_2SO_4}$
Eqn.	(3.12)	(3.12)	(3.13)	(3.14)
Temp. Range (K)	100-500	50-1000	50-1000	100-900
Coefficients				
a	28.98641	30.09200	3.259	3.8310×10^{4}
b	1.853978	6.832514	1.356×10^{-3}	1.119×10^{5}
c	-9.647459	6.793435	1.502×10^{-5}	4.209×10^{2}
d	16.63537	-2.534480	-2.374×10^{-8}	-4.73×10^{4}
e	0.000117	0.082139	1.056×10^{-11}	5.48×10^{2}

Equation (3.12) is obtained from the Nist Chemistry Webbook [26], Equation (3.13) is obtained from Poling et al. [28], and Equation (3.14) is obtained from Daubert et al. [27]. Values for liquid phase specific heat of $H_2SO_4{\cdot}H_2O$ solutions are tabulated in Zeleznik [37].

3.5 Transport Properties

Transport processes are those which occur due to gradients of, e.g., temperature, mass, or momentum. This asymmetry will cause a spontaneous flow of said temperature, mass, or momentum in order to reach a state of equilibrium. Thus, the transport properties describe the fluids response to these gradients. The model calls for viscosity, thermal conductivity and binary diffusion coefficients. Their values, under the conditions of this study ($z = 50$ km and the corresponding T_d and P_d), must be found for each pure component separately, and then properly combined. This is done

through the methods listed below. Mixtures are obtained using the appropriate mixing rules, Wilke's equation, and the Wassilijewa formula and are discussed in Section 3.6

3.5.1 Viscosity. The three main transport properties of a fluid include: thermal conductivity, diffusion coefficient, and viscosity, which arise due to gradients in temperature, molecular concentration, and momentum respectively. It can be thought of as a reflection of the microscopic molecular forces which arise as the fluid interacts with its boundaries moving at different velocities. It arises from Newton's second law as which relates the stress imparted onto the fluid to the fluid velocity gradient with respect to the boundary:

$$\tau = \eta \frac{\mathrm{d}v}{\mathrm{d}y} \tag{3.15}$$

In Equation (3.15) τ represents the shear stress tensor of a parcel of fluid, $\frac{\mathrm{d}v}{\mathrm{d}y}$ is the spatial velocity gradient along the y-axis for a fluid flowing along the x-direction, and η is the proportionality constant defined as the viscosity of the fluid in SI units of $\mathrm{Pa\,s}$.

Pure component viscosity values of the ambient atmosphere gases (i.e. CO_2 and N_2) are extracted from the NIST Chemistry Webbook [26] at the appropriate temperature and pressure corresponding to $z = 50$ km. The temperature dependence of water vapor viscosity is obtained from Daubert et al. [27]. The formula is given as:

$$\eta_{2v} = \frac{aT^b}{1 + \frac{c}{T} + \frac{d}{T^2}}, \tag{3.16}$$

where the constants a-d are given in Table 3.5. The formula for η_{2v} is valid for the temperature range $T \in [273.16, 1073.15]$ K with an error of $< 1\%$ reported by the author.

Vapor phase viscosity values for sulfuric acid are found through empirical formula given in Poling et al. [28]. Viscosity values are calculated from a dimensionless reduced viscosity, η_r, which is a function of the reduced temperature, $T_r = T/T_c$, defined as the ratio of the gas temperature to its critical temperature:

$$\eta_r = \eta\xi = f(T_r). \tag{3.17}$$

The term ξ is called the inverse viscosity, in $\mathrm{Pa}^{-1}\,\mathrm{s}^{-1}$, and has the form of:

$$\xi = 0.0176\left(\frac{T_c}{M^3 P_c^4}\right)^{1/6}. \tag{3.18}$$

The subscript c on the equations above represent critical values, and are available for many substances in Daubert et al. or the NIST Chemistry Webbook [27, 26]. The critical values for H_2SO_4 are given to be,
$T_c = 925$ K, $P_c = 64 \times 10^5$ Pa, $V_c = 177.03 \times 10^{-6}$ $\mathrm{m}^3\,\mathrm{mol}^{-1}$, which yield a reduced temperature of $T_r \approx 0.38$ and an inverse viscosity of $\xi_{1v} \approx 3.47 \times 10^4$ $\mathrm{Pa}^{-1}\,\mathrm{s}^{-1}$.

The determination of the function $f(T_r)$ is also given in Poling by Lucas [38], who suggests a form for $f(T_r)$ as:

$$f(T_r) = [a + b \cdot T_r^c - d \cdot \exp(e \cdot T_r) + f \exp(g \cdot T_r)] F_P^o F_Q^o \tag{3.19}$$

The percent error associated with Lucas's method are expected to be between 0.5-1.5% for nonpolar compounds and 2-4% for polar compounds, from experimental values [28].

Table 3.5. Constants for Equations (3.16) and (3.19).

Species	$\mathbf{H_2O}$	$\mathbf{H_2SO_4}$
Eqn.	(3.16)	(3.19)
Temp. Range (K)	273.16-1073.15	none
Coefficients		
a	6.1837×10^{-7}	0.018
b	6.7779×10^{-1}	0.807
c	8.4723×10^{2}	0.618
d	-7.3630×10^{4}	0.357
e	-	-0.449
f	-	0.340
g	-	-4.058

The constans a-g are given in Table 3.5, while F_P^o and F_Q^o are corrections factors. F_Q^o is only for the species He, H_2, and D_2, while F_P^o is dependant on the reduced dipole moment μ_r^{dip}, defined to be:

$$\mu_r^{dip} = 52.46 \frac{\left(\mu^{dip}\right)^2 P_c}{T_c^2} \tag{3.20}$$

where μ^{dip} represents the dipole moment and has an approximate value of $\mu_1^{dip} \approx 2.725$ Debye for sulfuric acid (with unknown accuracy by author) [27]. For the

given parameter values, we obtained a reduced sulfuric acid dipole moment of $\mu_{1r}^{dip} \approx 0.029$, which we can then use to obtain a value for the correction F_P^o:

$$F_P^o = 1 + 30.55(0.292 - Z_c)^{1.72} \tag{3.21}$$

The formula for F_P^o is exclusively for reduced dipole values in the range of $0.022 \leq \mu_r^{dip} \leq 0.075$ and Z_c is the critical compressibility defind as:

$$Z_c = \frac{P_c V_c}{R T_c} \tag{3.22}$$

For sulfuric acid, the critical compressibility is $Z_c \approx 0.1473$. We obtained a value for the correction factor as $F_P^o \approx 2.10$. Finally, solving Equation (3.17) for η, we obtain a value for the pure component sulfuric acid gas viscosity as $\eta_{1v} \approx 1.42 \times 10^{-5}$ Pa s.

3.5.2 Thermal Conductivity. The coefficient of thermal conductivity appears as the proportionality constant in Fourier's law of thermal conduction, which relates a flux of heat to the local temperature gradient. In one dimension:

$$q = -\lambda \frac{\mathrm{d}T}{\mathrm{d}x}, \tag{3.23}$$

where q is the heat flux density in $\mathrm{W\,m^{-2}}$, T is the local temperature in K, and λ is the coefficient of thermal conductivity in $\mathrm{W\,m^{-1}\,K^{-1}}$.

Pure component thermal conductivity values of the ambient atmosphere gases (i.e. CO_2 and N_2) are extracted from the NIST Chemistry Webbook [26] at the appropriate temperature and pressure corresponding to $z = 50$ km. The temperature dependence of water vapor thermal conductivity is given in Pruppacher et al. [21]. The formula is given as:

$$\lambda_{2v} = (3.78 + 0.020 \cdot T)\left(\frac{1}{2.39}\right) \times 10^{-2} \tag{3.24}$$

where T is the gas temperature in units of degrees celsius and λ_{2v} has units of $\mathrm{W\,m^{-1}\,K^{-1}}$.

Vapor phase thermal conductivity for sulfuric acid is found in Poling et al. [28], through empirical formula using the methods of Chung et al. [39]. The formula has the form:

$$\frac{\lambda M}{\eta C^v} = \frac{3.75\Psi}{C^v/R}. \tag{3.25}$$

The term on the left hand side is know as the Eucken factor, it relates the thermal conductivity to viscosity and is dimensionless. The variables λ, η, M, C_v, R represent the thermal conductivity, viscosity obtained in section 3.5.1, molar mass, isochoric specific heat, and the universal gas constant respectively. Ψ is a function of temperature and contains factors which are dependant upon whether the gas is polar or not. It has the form:

$$
\begin{aligned}
\Psi &= 1 + \frac{\alpha[0.215 + 0.28288\alpha - 1.061\beta + 0.26665Z]}{[0.6366 + \beta Z + 1.061\alpha\beta]} \\
\alpha &= \frac{C^v}{R} - 3/2 \\
\beta &= \frac{1}{1.32} \\
Z &= 2 + 10.5T_r^2
\end{aligned} \tag{3.26}
$$

The β term has a specific value for each polar compound. Values for β can be found for a limited number of gases in Chung et al. [39], but are not available for sulfuric acid. Thus, it is suggested by the authors that for polar compounds without a value for β use a default value of $\beta = (1.32)^{-1}$. The quantity T_r in Z is again the reduced temperature given in section 3.5.1. To obtain α we use the relation $C^v = C^p - R$. We obtain $\Psi \approx 3.32$, then solving Equation (3.25) for λ we obtained the thermal conductivity for sulfuric acid vapor as $\lambda_{1v} \approx 1.50 \times 10^{-2} \mathrm{W\,m^{-1}\,K^{-1}}$. Errors associated with this method typically lie between 5-7% for nonpolar compounds, and larger for polar compounds [28].

Temperature dependence of liquid phase water vapor and sulfuric acid thermal conductivity is given in Daubert at. al. [27]. They are both obtained from a polynomial expansion of the form:

$$
\lambda_{(1,2)\ell} = a + bT + cT^3 + dT^4. \tag{3.27}
$$

with T in kelvin and the coefficients are given in Table 3.6. The percent error associated with Equation (3.27) for water is less than 1%, and for sulfuric acid is less than 3% [27].

Table 3.6. Constants for Equation (3.27).

Species	$\mathbf{H_2O}$	$\mathbf{H_2SO_4}$
Eqn.	(3.27)	(3.27)
Temp. Range (K)	273.16-633.15	273.59-371.32
Coefficients		
a	-4.3200×10^{-1}	0.0142
b	5.7255×10^{-3}	1.0763×10^{-3}
c	-8.0780×10^{-6}	-
d	1.8610×10^{-9}	-

3.5.3 Diffusion Coefficient. The diffusion coefficient is a measure of the ability of either a gas or fluid with a gradient in concentration, to restore an equal spatial partition between molecules. It becomes present in Fick's law, which states that the molecular concentration flux J, in one dimension, is proportional to the negative of the gradient in molecular concentration. Mathematically, Fick's law reads:

$$J = -D\frac{\mathrm{d}\varphi}{\mathrm{d}x} \tag{3.28}$$

Where J is the diffusion flux in $\mathrm{mol\,m^{-2}\,s^{-1}}$, φ is the concentration in $\mathrm{mol\,m^{-3}}$, and the proportionality constant D represents the diffusion coefficient in units of $\mathrm{m^2\,s^{-1}}$. Values for the diffusion coefficient are obtained through the use of a formula with empirical relations, based on experimental measurements, and derived from theoretical solutions to the Boltzmann equation [28]. The diffusion coefficient for a

binary gas mixtures with components A and B at low pressures, has the formula:

$$D_{AB} = \frac{0.00143 \cdot T^{1.75}}{P\sqrt{M_{AB}}} \frac{1}{\left[(\Sigma_v)_A^{1/3} + (\Sigma_v)_B^{1/3}\right]}. \tag{3.29}$$

This formula is suggested by Fuller et al. [40]. The variables T, P, M_{AB}, represent the temperature, pressure, and the harmonic mean of the molecular masses. The term $(\Sigma_v)_{A/B}$ is found for each component by summing atomic diffusion volumes increments, given in reference [28] and the averaged molecular mass is given by the formula:

$$M_{AB} = \frac{2}{(1/M_B) + (1/M_B)} \tag{3.30}$$

The atomic volume increments needed for Equation (3.29) are given in the Table 3.7 for species pertinent to Venus' atmosphere.

Table 3.7. Atomic diffusion volumes for species found on Venus.

Atomic Diffusion Volume Increments	
H	2.31
O	6.11
S	22.9
Diffusion Volumes of Venus Species (Σ_v)	
CO_2	26.9
H_2SO_4	51.96
H_2O	13.1

It is important to note, that the diffusion coefficient's components (A and B) are in reference to the vapor to be diffused (component B) into the ambient host gas (component A). Since Venusian clouds are aqueous sulfuric acid, the vapor phase is

composed of water as well as sulfuric acid. It is then necessary to compute two diffusion coefficients: one for water vapor, and another for sulfuric acid vapor. The diffusion of sulfur trioxide from the dissociation of the vaporous sulfuric acid is ignored for simplicity.

The ambient gas is taken to be only carbon dioxide since it occupies over 96% of the atmosphere. The diffusion coefficients for sulfuric acid and water in CO_2 are computed as $D_{acid} \approx 1.08 \times 10^{-5}\ \mathrm{m^2\,s^{-1}}$ and $D_{water} \approx 2.79 \times 10^{-5}\ \mathrm{m^2\,s^{-1}}$. The average percent error reported by Poling is approximately 5.4%, when comparing results from Equation (3.29) to experimental values.

3.6 Mixtures

One of the most important treatments of the thesis is given to mixtures. Since the clouds of Venus are aqueous sulfuric acid, we have a binary mixture of pure sulfuric acid and water. The vapor phase is also a combination of acid and water, as well as sulfur trioxide from the dissociation of acid [31].

As noted earlier, the gas total pressure follows Dalton's law, is the sum of the partial pressures $p_g = p_v + p_d$. By extensions, the pressure of the vapor phase and dry atmospheric pressure are the sum of their components partial pressure, e.g. $p_v = p_1 + p_2 + p_3$. The total density of the gaseous phase follows mass conservation and is the sum of its components, $\rho_g = \rho_v + \rho_d$. Again, the pure component vapor densities and ambient densities add to form the vapor and dry ambient mixture densities.

The molecular weight of a mixture, $\overline{M}$, can be found, interchangeably, either as a weighted sum by mole χ_i fractions, or by a weighted inverse sum by mass fractions w_i,

$$\overline{M} = \sum_i \chi_i \cdot M_i = \left[\sum_i \frac{w_i}{M_i} \right]^{-1}. \tag{3.31}$$

Heat capacity mixtures are obtained by a simple weighted sum of specific heats by the mixtures component weight fractions.

$$C^m = \sum_{i=1}^{n} w_i C_i \tag{3.32}$$

It is an easy exercise to show for a two component mixture of dry gas and vapor (given by the subscripts d and v respectively), that the heat capacity of the mixture can be rewritten in the form:

$$\begin{aligned} C^m &= C_d \frac{1 + x_{mv} r}{1 + x_{mv}} \\ r &= \frac{C_v}{C_d} \\ x_{mv} &= \frac{\rho_v}{\rho_d}. \end{aligned} \tag{3.33}$$

The viscosity of a gas mixture is obtained from Poling et al. [28]. The mixture viscosity as well as thermal conductivity is found from pure values obtained through the methods in the previous sections, and are combined using Wilke's method [41].

$$\eta_m = \sum_{i=1}^{n} \frac{\chi_i \eta_i}{\sum_{j=1}^{n} \chi_j \phi_{ij}} \tag{3.34}$$

where

$$\phi_{ij} = \frac{\left[1 + (\eta_i/\eta_j)^{1/2}(M_j/M_i)^{1/4}\right]^2}{[8(1 + M_i/M_j)]^{1/2}}. \tag{3.35}$$

Thus, for n pure components, each with viscosity η_i and molar mass M_i, the mixture viscosity is given above. Wilke's formula must be applied in order to obtain mixture viscosities for: (1) the ambient gas (CO_2 and N_2), (2) the vapor phase (H_2SO_4 and H_2O), and (3) the gaseous phase, which is a mixture of the ambient and vapor. Values for the dry, vapor and gaseous phase viscosity mixtures are calculated to be, $\eta_d \approx 1.78 \times 10^{-5}$ Pa s, $\eta_v \approx 1.33 \times 10^{-5}$ Pa s and $\eta_g \approx 1.76 \times 10^{-5}$ Pa s. The percent errors reported by Poling for Equation (3.34) are less than 1% for nonpolar gas mixtures, while errors for polar-polar gas mixtures are not quantitatively discussed [28].

The empirical formula used to combine low pressure gas thermal conductivities in a gaseous mixture, is analogous to the theoretical relation for mixture viscosity given by Equation (3.34):

$$\lambda_m = \sum_{i=1}^{n} \frac{\chi_i \lambda_i}{\sum_{j=1}^{n} \chi_j A_{ij}}. \tag{3.36}$$

The empirical Equation (3.36) is referred to as the Wassilijewa equation. A suggested form for A_{ij} is given by Mason and Saxena [42]:

$$A_{ij} = \frac{\epsilon\Big[1 + (\lambda_i/\lambda_j)^{1/2}(M_j/M_i)^{1/4}\Big]^2}{[8(1 + M_i/M_j)]^{1/2}}. \tag{3.37}$$

In the above equation, λ_i, M_i represent the thermal conductivity and molar mass of the ith gas mixture component, while ϵ is a constant near 1. In this thesis I will follow the author's lead and use $\epsilon = 1$. From the pure component thermal conductivities given in the NIST Chemistry Webbook, values for dry air and humid air thermal conductivities are found to be, $\lambda_d \approx 2.20 \times 10^{-2}$ and $\lambda_g \approx 2.16 \times 10^{-2}$ $\mathrm{Wm^{-1}K^{-1}}$. Percent errors between Equation (3.36) and experimental values are greater than 5-8% for polar-polar and polar-nonpolar gas mixtures. While nonpolar gas mixtures are found to have errors typically less that 3-4% [28].

The model input parameters, calculated from the equations in this chapter, are summarized in Table 3.8.

Table 3.8. Calculated model input parameters.

Parameter	Value	Units
L	1.66×10^{4}	$\mathrm{J\,kg^{-1}}$
p_v	33.46	Pa
p_g	107033	Pa
ρ_v	3.90×10^{-4}	$\mathrm{kg\,m^{-3}}$
ρ_g	1.59	$\mathrm{kg\,m^{-3}}$
ρ_ℓ	1.82×10^{3}	$\mathrm{kg\,m^{-3}}$
C_d^p	38.90	$\mathrm{J\,kg^{-1}\,K^{-1}}$
C_v^p	45.21	$\mathrm{J\,kg^{-1}\,K^{-1}}$
C_g^p	38.90	$\mathrm{J\,kg^{-1}\,K^{-1}}$
C_ℓ^p	60.40	$\mathrm{J\,kg^{-1}\,K^{-1}}$
η_d	1.78×10^{-5}	Pa s
η_v	1.33×10^{-5}	Pa s
η_g	1.76×10^{-5}	Pa s
λ_d	0.030	$\mathrm{W\,m^{-1}\,K^{-1}}$
λ_v	0.022	$\mathrm{W\,m^{-1}\,K^{-1}}$
λ_g	0.030	$\mathrm{W\,m^{-1}\,K^{-1}}$
λ_ℓ	0.39	$\mathrm{W\,m^{-1}\,K^{-1}}$
D_{acid}	1.08×10^{-5}	$\mathrm{m^2\,s^{-1}}$
D_{water}	2.79×10^{-5}	$\mathrm{m^2\,s^{-1}}$

Chapter 4: Results

Predictions for the intrinsic acoustic attenuation coefficient and dispersion in the Venus cloud layer are given in Figures 4.1 and 4.2 respectively. The overall attenuation spans approximately 5 orders of magnitude across the plotted frequency range. The curves were generated using parameters at an altitude of $z = 50$ km (Table 3.1), a cloud density of 80% ρ_{cl}, and thermodynamic/transport mixture variables tabulated in Table 3.8 with mode 3 as the mean particle radius. The dashed vertical lines represent the characteristic frequencies from Table 2.1, where $f_{D1,2}$ is the phase change frequency of species 1, H_2SO_4, and 2, H_2O, and f_ν is the frequency of momentum transfers. The locations of the characteristic frequencies are where attenuation due to the respective mechanisms is dominant. Two inflection points are distinguished in the attenuation and sound speed curves, at the characteristic frequencies f_{D2} and f_ν. The three characteristic frequencies (f_{D1}, f_{D2}, and f_ν) indicate the presence of special relaxation times associated with phase changes and momentum transfer, as discussed in Section 2.2. Thus, losses due to phase changes dominate for frequencies < 100 Hz. Above this, absorption due to momentum transfers become dominant. The overall intrinsic dispersion is very small ($\sim 10^{-2}$ %), across the given frequency range. For frequencies between $10^{-3} - 10^{-1}$ Hz, the dispersion is sensitive to relatively small frequency changes in the phase change dominant region. Above this, the sound speed is mostly unaffected, hence, the presence of atmospheric clouds has negligible effects on the intrinsic dispersion.

Figure 4.1. Frequency dependence of the attenuation coefficient α in the atmosphere of Venus ($z = 50$ km)

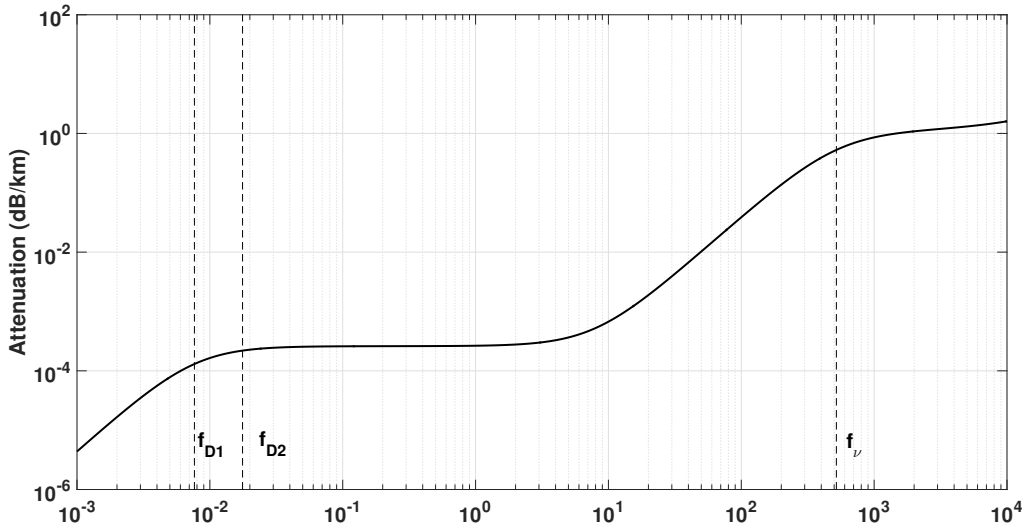

Figure 4.2. Frequency dependence of sound speed in the atmosphere of Venus ($z = 50$ km)

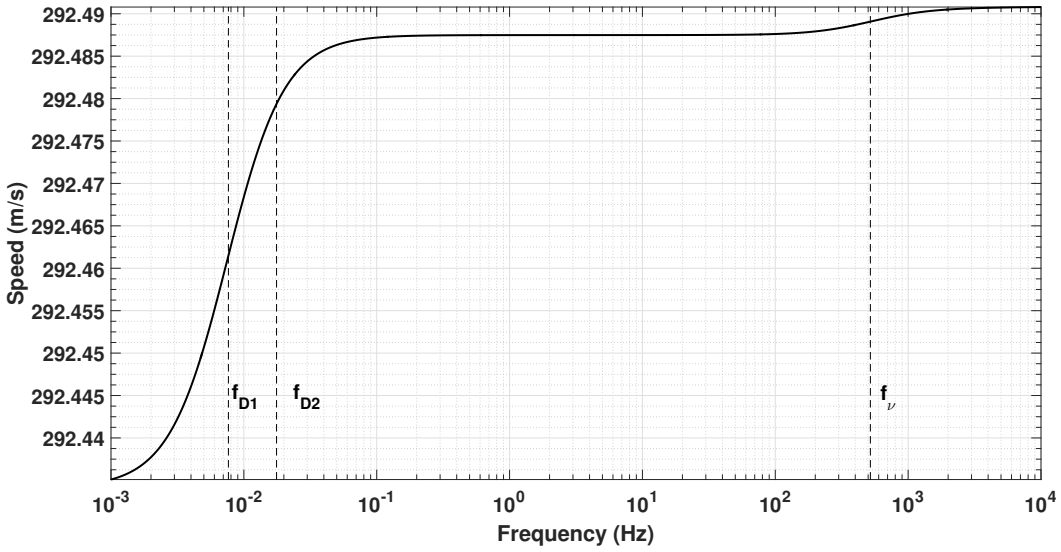

The dependence of the attenuation and dispersion on the mean liquid particle radius is given in Figures 4.3 and 4.4. The plots were generated for the same atmospheric conditions as Figures 4.1 and 4.2. For an increase in droplet radius, the absorption coefficient decreases, and thus is inversely dependent upon the droplet size. Additionally, the characteristic frequencies, f_{D1}, f_{D2} and f_{ν}, are inversely proportional to the square of the droplet radius, and thus the peak attenuation per wavelength occurs at earlier frequencies for increasing droplet size.

As for the sound speed, a change in mean droplet radius shifts the location of the dispersion to lower frequencies. The overall change in sound speed remains approximately the same.

Figure 4.3. Frequency dependence of the attenuation coefficient for different values of the cloud mean particle radii (modes)

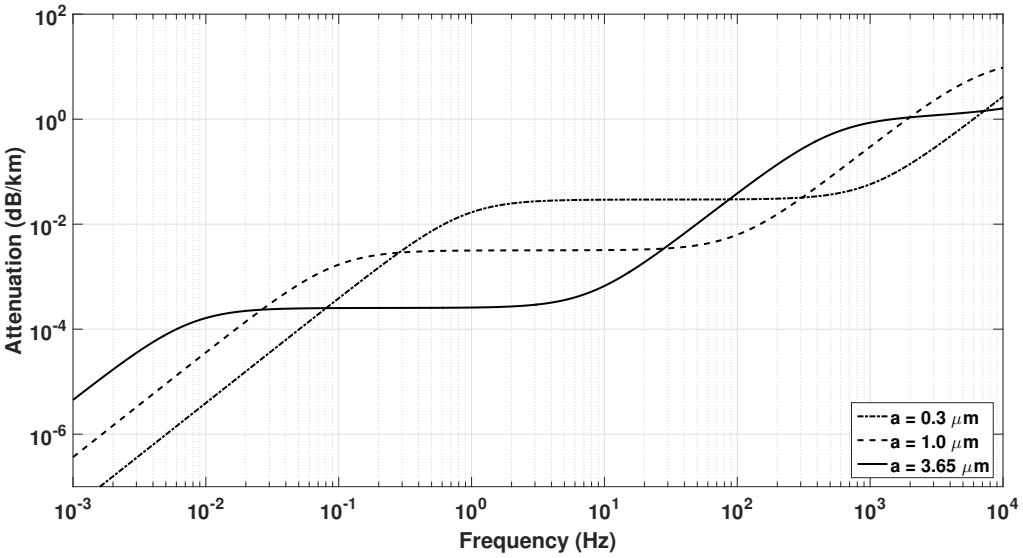

The influence of cloud particle density on the attenuation coefficient and sound speed is given in Figures 4.5 and 4.6. The plots were generated for the same

Figure 4.4. Frequency dependence of the sound speed for different values of the cloud mean particle radii (modes)

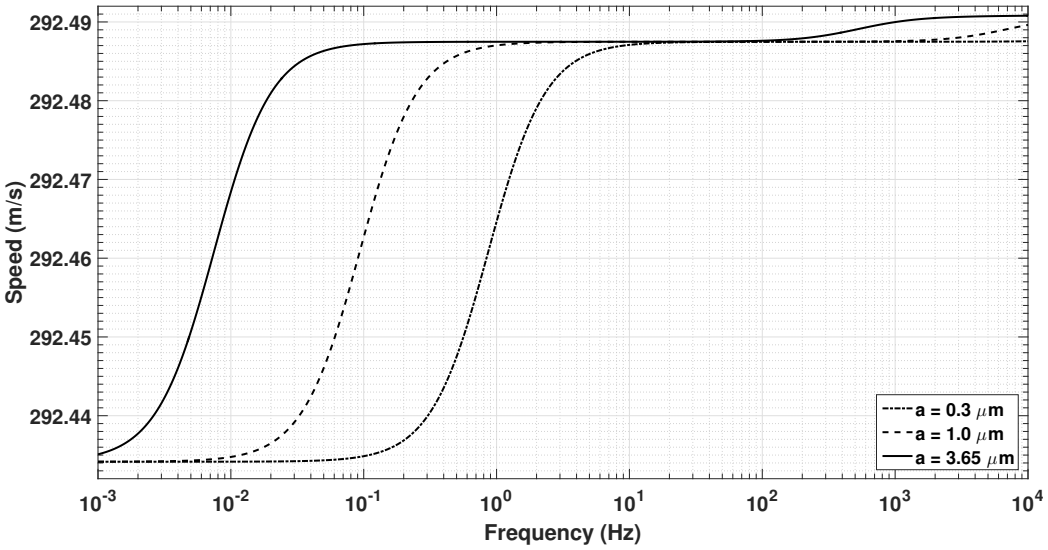

atmospheric conditions as Figures 4.1 and 4.2, with mean particle size corresponding to mode 3 ($a = 3.65\ \mu m$). The cloud density refers to the total mass of the condensates in a given volume of atmosphere (atmosphere plus droplets). Figure 4.5 gives the attenuation coefficient for different values of cloud density, which are decreased by factors of 1/2. As the cloud density is decreased, so too are the number of absorbers and thus the absorption of sound. However, the characteristic frequency of phase change f_{D1} and f_{D2} is dependent on the amount of liquid m. Hence we see for smaller cloud densities, and thus smaller m, the characteristic frequency of phase changes also decreases while the momentum characteristic frequency does not.

The influence of cloud density on the dispersion shifts the dispersion to lower frequencies with decreasing density. At the same time, the dispersion above 1000 Hz (due to momentum transfer) is flattened by the upward shifting speed profile.

Figure 4.5. Frequency dependence of the attenuation coefficient for different cloud densities

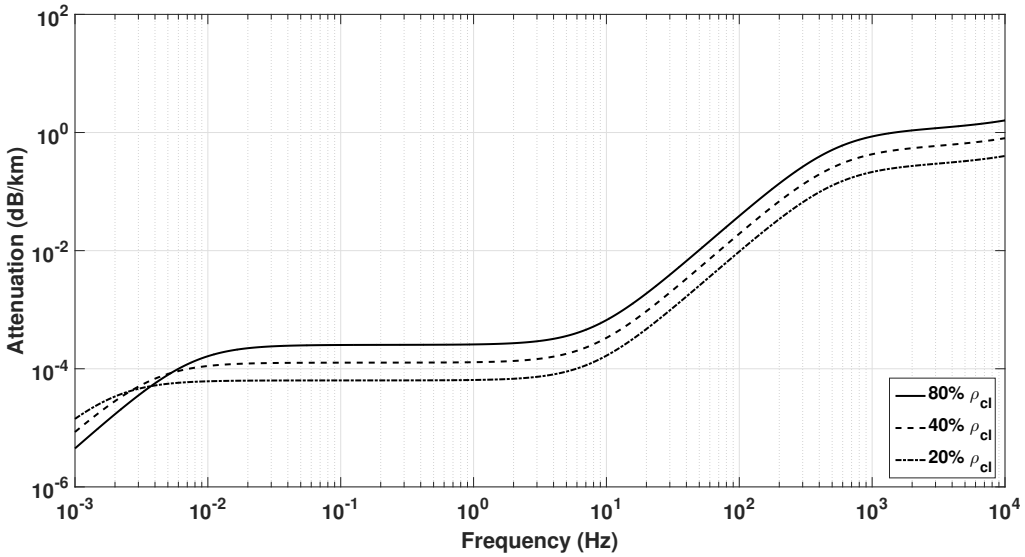

Figure 4.6. Frequency dependence of the sound speed for different cloud densities

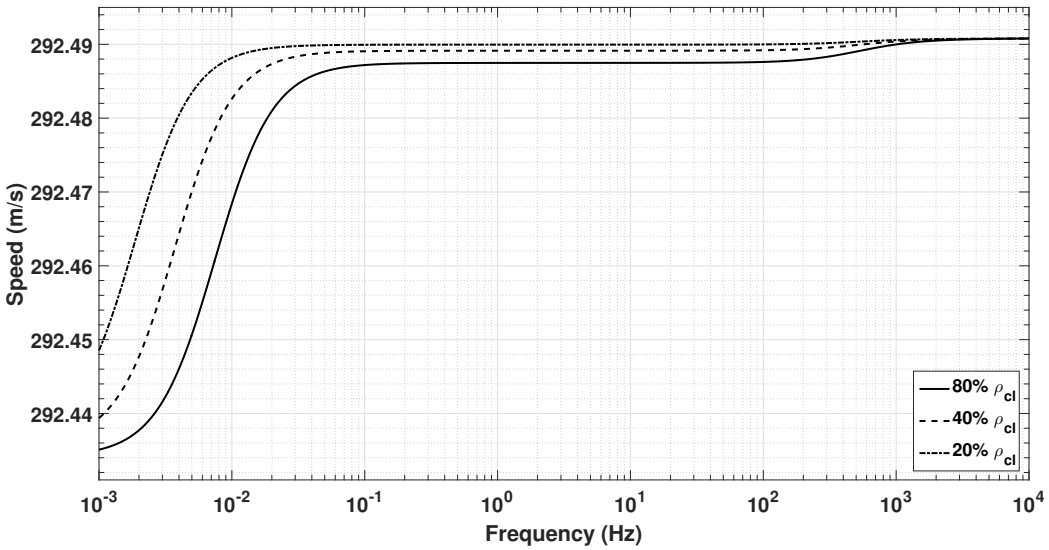

Chapter 5: Discussion and Conclusion

The effects of clouds on the propagation of low frequency sound has been investigated on Venus. Predictions for the attenuation coefficient and intrinsic dispersion, obtained from the complex acoustic wavenumber, have been presented for low frequencies. The predictions show that the effect of clouds on the absorption and dispersion is dominated by phase change effects (controlled by diffusion) of the liquid droplets in the infrasonic range. At higher frequencies, momentum and thermal transfers are the dominant source of attenuation, but affect the dispersion very little.

The ambient conditions and properties of the cloud layer satisfy the assumptions made in the model at 50 km altitude. The presence of aqueous sulfuric acid droplets, $H_2SO_4 \cdot H_2O$, necessitates the use of mixing rules when calculating model input parameters (i.e. thermodynamic properties, transport properties, etc.). The effects of varying the mean droplet size show an increase in absorption with a decrease in droplet size, for a given cloud density. The overall dispersion across the frequency range of interest changes negligibly ($\sim 10^{-3}\%$) with the mean droplet size. However, the frequency location where the dispersion occurs, is shifted to lower frequencies with increasing droplet size.

A maximum cloud density is taken to be $\rho_{cl} \approx 4.5 \times 10^{-5}$ kg m^{-3}, which is without considering cloud dynamics or precipitation. However, since the cloud density is known to be highly spatially and temporally variable, the attenuation and dispersion dependence on cloud density is investigated. The absorption is shown to decrease with cloud density, as well as the frequencies associated with phase change, f_{D1} and f_{D2}, as

they are proportional to the liquid content m. The overall change in dispersion with cloud density is negligible.

5.1 Future Work

The predictions given in this thesis are limited to the low frequency region. In order to expand the frequency domain, real gas effects can no longer be ignored. Thus, a natural extension to the model would include the use of a non ideal equation of state to account for molecular relaxation effects. The work of Petculescu [2] gives generic predictions for acoustic dispersion and absorption of the ambient Venusian atmosphere using the van der Waals equation of state. Hence, combining the effects of phase changes at low frequencies (this work) and real gas effects from Petculescu, would give a more complete picture of the acoustic profile of Venus' atmosphere across a much larger frequency range and in the presence of clouds.

Additionally, the presence of winds within the cloud layer will have to be analyzed within the context of the model, as they can reach maximum speeds of 100 $\mathrm{m\,s^{-1}}$ in the upper cloud layer. The plane-wave approximation will also need to be reviewed. For low frequency waves ($f \sim 10^{-2}$ Hz and below), this corresponds to wavelengths as small as 30 km. At these wavelengths, the cloud properties (temperature, density, pressure, etc.) change appreciably and will therefore considerably modify sound propagation.

Bibliography

[1] C. A. Jones, D. C. Arney, G. Z. Bassett, J. R. Clark, A. I. Hennig, and J. C. Snyder, "High altitude venus operational concept (havoc): Proofs of concept," , NASA (2015), https://ntrs.nasa.gov/search.jsp?R=20160006580&hterms=arney+HAVOC+HAVOC&qs=N%3D0%26Ntk%3DAll%7CAuthor-Name%26Ntt%3DHAVOC%7Carney%26Ntx%3Dmode%2520matchallpartial%7Cmode%2520matchall%26Nm%3D123%7CCollection%7CNASA%2520STI%7C%7C17%7CCollection%7CNACA.

[2] A. Petculescu, "Acoustic properties in the low and middle atmospheres of mars and venus," J. Acoust. Soc. Am. **140**(2), 1439–1446 (2016).

[3] M. Baudoin and F. Coulouvrat, "Sound, infrasound, and sonic boom absorption by atmospheric clouds," J. Acoust. Soc. Am. **130**(3), 1142–1153 (2011).

[4] T. M. Donahue and C. T. Russell, "The venus atmosphere and ionosphere and their interaction with the solar wind: An overview," in *Venus II: Geology, Geophysics, Atmosphere, and Solar Wind Environment*, edited by S. Bougher, D. Hunten, and R. Phillips (The University of Arizona Press, Reading, Massachusetts, 1997), pp. 3–32.

[5] Information on the exploration history of Venus is available at https://solarsystem.nasa.gov/planets/venus/exploration/?page=0&per_page=10&order=launch_date+desc%2Ctitle+asc&search=&tags=Venus&category=129#ancient-observers (Last viewed November 1, 2018).

[6] S. Tellmann, M. Patzold, B. Hausler, M. K. Bird, and G. L. Tyler, "Structure of the venus neutral atmosphere as observed by the radio science experiment vera on venus express," J. Geophys. Res., **114** (2009).

[7] A. Sánchez-Lavega, R. Hueso, G. Piccioni, P. Drossart, J. Peralta, S. Pérez-Hoyos, C. F. Wilson, F. W. Taylor, K. H. Baines, D. Luz, S. Erard, and S. Lebonnois, "Variable winds on venus mapped in three dimensions," Geophys. Res. Lett. **35**, L13204 (2008).

[8] JAXA, "Venus climate orbiter akatsuki / planet-c, http://www.stp.isas.jaxa.jp/venus/top_english.html," (2009), information on the Akatsuki mission is available athttp://www.stp.isas.jaxa.jp/venus/top_english.html.

[9] A. Sánchez-Lavega, *An introduction to Planetary Atmospheres* (Taylor and Francis Group, LLC, Boca Raton, Florida, 2011).

[10] L. W. Esposito, J.-L. Bertaux, V. Krasnopolsky, V. I. Moroz, and L. V. Zasova, "Chemistry of lower atmosphere and clouds," in *Venus II: Geology, Geophysics, Atmosphere, and Solar Wind Environment*, edited by S. Bougher, D. Hunten, and

R. Phillips (The University of Arizona Press, Reading, Massachusetts, 1997), pp. 3–32.

[11] K. McGouldrick, O. B. Toon, and D. H. Grinspoon, "Sulfuric acid aerosols in the atmosphere of the terrestrial planets," Planetary and Space Science **59**, 934–941 (2011).

[12] T. Imamura and G. L. Hashimoto, "Venus cloud formation in the meridional circulation," J. Geophys. Res. **103**, 31,349–31,336 (1998).

[13] E. P. James, O. B. Toon, and G. Schubert, "A numerical microphysical model of the condensational venus cloud," Icarus **129**(IS975763), 147–171 (1997).

[14] T. Imamura and G. L. Hashimoto, "Microphysics of venusian clouds in rising tropical air," J. Atmos. Sci. **58**, 3,597–3,612 (2001).

[15] A. Young, "Are the clouds on venus sulfuric acid?," Icarus **18**, 564—582 (1973).

[16] J. B. Pollack, D. W. Strecker, F. C. Witteborn, E. F. Erickson, and B. J. Baldwin, "Properties of the clouds of venus, as inferred from airborne observations of its near-infrared reflectivity spectrum," Icarus **34**, 28–45 (1978).

[17] J. W. Hansen, J. E.and Hovenier, "Interpretation of the polarization of venus," J. Atmos. Sci. **31**, 1137—1160 (1974).

[18] R. G. Knollenberg and D. M. Hunten, "The microphysics of the clouds of venus: Results of the pioneer venus particle size spectrometer experiment," J. Geophys. Res. **85**, 8039–8058 (1980).

[19] H. E. Bass, L. C. Sutherland, J. Piercy, and L. Evans, "Absorption of sound by the atmosphere," in *Physical Acoustics*, edited by W. Mason and R. Thurston, Vol. 17 (Academic Press Inc., Orlando, Florida 32887, 1984), Chap. 3, pp. 145–232.

[20] D. A. Gubaidullin and R. I. Nigmatullin, "On the theory of acoustic waves in polydispersed gas-vapor-droplet suspensions," International Journal of Multiphase Flow **26**, 207–228 (2000).

[21] H. R. Pruppacher and J. D. Klett, *Microphysics of Clouds and Precipitation* (D. Reidel Publishing Company, Hingham, Massachusetts 02043, 1978).

[22] A. M. Mood, F. A. Graybill, and D. C. Boes, *Introduction to the Theory of Statistics.*, 3rd ed. (McGraw-Hill, New York, 1974).

[23] S. Temkin and R. A. Dobbins, "Attenuation and dispersion of sound by particulate-relaxation processes," J. Acoust. Soc. Am. **40**, 317–324 (1966) doi: `https://doi.org/10.1121/1.1910073`.

[24] F. E. Marble and D. C. Wooten, "Sound attenuation in a condensing vapor," Phys. Fluids **13**(11), 2657–2664 (1970).

[25] G. A. Davidson, "Sound propagation in fogs," J. Atmos. Sci. **32**(11), 2201–2205 (1975).

[26] P. Linstrom and W. Mallard, *NIST Chemistry WebBook, NIST Standard Reference Database Number 69* (National Institute of Standards and Technology, Gaithersburg MD, 20899, 1997), `https://doi.org/10.18434/T4D303`, (retrieved November 14, 2018).

[27] T. E. Daubert, R. P. Danner, and J. P. O'Connell, *The Properties of Gases and Liquids*, 5th ed. (McGraw-Hill, New York, 2001).

[28] B. E. Poling, J. M. Prausnitz, and J. P. O'Connell, *The Properties of Gases and Liquids*, 5th ed. (McGraw-Hill, New York, 2001).

[29] G. P. Ayers, R. W. Gillett, and G. L. Gras, "On the vapor pressure of sulfuric acid," Geophys. Res. Lett. **7**, 433–436 (1980).

[30] M. Kulmana and A. Laaksonen, "Binary nucleation of water-sulfuric acid system: Comparison of classical theories with different h2so4 saturation vapor pressures," J. Chem. Phys **93**(1), 696–701 (1990).

[31] J. I. Gmitro and T. Vermeulen, "Vapor-liquid equilibria for aqueous sulfuric acid," A.I.Ch.E. 740–746 (1964).

[32] E. Chassefière, O. Korablev, T. Imamura, K. H. Baines, C. F. Wilson, D. V. Titov, K. L. Aplin, T. Balint, J. E. Blamont, C. G. Cochrane, C. Ferencz, F. Ferri, M. Gerasimov, J. J. Leitner, J. Lopez-Moreno, B. Marty, M. Martynov, S. V. Pogrebenko, A. Rodin, J. A. Whiteway, L. V. Zasova, J. Michaud, R. Bertrand, J.-M. Charbonnier, D. Carbonne, P. Raizonville, and EVE team, "European venus explorer (eve): an in-situ mission to venus," Experimental Astronomy **23**(3), 741–760 (2009) `https://doi.org/10.1007/s10686-008-9093-x` doi: `10.1007/s10686-008-9093-x`.

[33] I. W. Eames, N. J. Marr, and H. Sabir, "The evaporation coefficient of water: a review," Int. J. Heat Mass Transfer **40**(12), 2963–2973 (1997).

[34] D. H. Grinspoon, J. B. Pollack, B. R. Sitton, R. W. Carlson, L. W. Kamp, K. H. Baines, T. Encrenaz, and F. W. Taylor', "Probing venus's cloud structure with galileo nims," Planet. Space Sci. **4**(7), 515–542 (1993).

[35] C. D.Parkinson, P. Gao, R. Schulte, S. W. Bougher, Y. L. Yung, C. G. Bardeen, V. Wilquet, A. C. Vandaele, A. Mahieux, S. Tellmann, and M. Patzold, "Distribution ofsulphuric acid aerosols in the clouds and upper haze of venus using venus express vast and vera temperature profiles," Planetary and Space Science **113-114**, 205–218 (2015).

[36] A. Sánchez-Lavega, S. Pérez-Hoyos, and R. Hueso, "Clouds in planetary atmospheres: A useful application of the clausius-clapeyron equation," Am. J. Phys. **72**(6), 767–774 (2004).

[37] F. J. Zeleznik, "Thermodynamics properties of the aqueous sulfuric acid system to 350k," J. Phys. Chem. Ref. Data **20**, 1157–1200 (1991).

[38] K. Lucas, "Phase equilibria and fluid properties in the chemical industry," DECHEMA; Frankfurt 573 (1980).

[39] T. H. Chung, M. Ajlan, L. L. Lee, and K. E. Starling, "Generalized multiparameter correlation for nonpolar and polar fluid transport properties," Ind. Eng. Chem. Res. **27**, 671 (1988).

[40] E. N. Fuller, K. Ensley, and J. C. Giddings, "Diffusion of halogenated hydrocarbons in helium. the effect of structure on collision cross sections," The Journal of Physical Chemistry **73**(11), 3679–3685 (1969) https://doi.org/10.1021/j100845a020 doi: 10.1021/j100845a020.

[41] C. R. Wilke, "A viscosity equation for gas mixtures," J. Chem. Phys. **18**, 517 (1950).

[42] E. A. Mason and S. C. Saxena, "Approximate formula for the thermal conductivity of gas mixtures," The Physics of Fluids **1**, 361 (1958).

Trahan, Adam J. Bachelor of Science in Physics, University of Louisiana at Lafayette, Spring, 2016; Master of Science in Physics, University of Louisiana at Lafayette, Fall 2018.
Major: Physics
Title of Thesis: Acoustic Attenuation in the Lower Cloud Layer of Venus
Thesis Director: Andi Petculescu
Pages in Thesis: 75; Words in Abstract: 260

Abstract

Generic predictions for the acoustic wavenumber at low frequencies in the condensational cloud layers of Venus are presented, based on and adapted from the terrestrial model of Baudoin *et al.* (J. Acoust. Soc. Am. **130**. 1142 (2011)). While the general thermodynamics of Earth clouds is well understood, that of Venusian clouds is still a matter of debate. Venus' clouds are primarily formed of H_2O and H_2SO_4 vapors and aqueous sulfuric acid droplets, the fluxes of which are not fully constrained due to the few in situ observations. Inside the clouds, the Navier-Stokes-Fourier equations of continuum fluid mechanics are used for the gaseous (dry + vapor) and liquid phases of H_2O andH_2SO_4, combined with equations describing the evaporation/condensation processes; the gaseous phase is treated as an ideal gas and the liquid droplets are considered polydisperse. Thermophysical parameters are interpolated at the ambient conditions pertaining to an altitude of 50 km, a level where balloon platforms (e.g., European Space Agency's EVE) and manned airships (e.g., NASA's HAVOC) may be deployed in the future. At low frequencies, the dominant source of absorption is caused by the evaporation/condensation of the liquid phase. At higher frequencies, absorption is dominated by momentum transfers between the wave and the ambient gas and liquid droplets. The intrinsic dispersion is negligible. Sensitivity studies of the attenuation

coefficient and the sound speed on the cloud physical parameters is performed, namely, the mean cloud particle size and the cloud density. The attenuation coefficient is sensitive to changes in both mean cloud particle size and cloud density, while the intrinsic dispersion changes negligibly.

Biographical Sketch

Adam J. Trahan was born on December 31, 1990. He is a native of Abbeville Louisiana, son to Nancy Duhon, and has spent his life residing in south Louisiana. He attended the University of Louisiana at Lafayette where he received his Bachelor of Science degree in the spring of 2016 with a double major in physics and mathematics. During his undergraduate career, he was accepted into the Naval Research Enterprise Internship Program (NREIP), where he spent the summer of 2015 performing research in structural materials at the Naval Surface Warfare Center, MD. He was then accepted into the Graduate Program at the University of Louisiana at Lafayette, where he received his Master of Science degree in physics in the Fall of 2018.